Formation of Highly Oxygenated Low-Volatility Products from Cresol Oxidation

Rebecca H. Schwantes[1,4], Katherine A. Schilling[2,5], Renee C. McVay[2,6], Hanna Lignell[2,7], Matthew M. Coggon[2,6], Xuan Zhang[1,8], Paul O. Wennberg[1,3], and John H. Seinfeld[2,3]

[1]Division of Geological and Planetary Sciences, California Institute of Technology, Pasadena, California 91125, United States
[2]Division of Chemistry and Chemical Engineering, California Institute of Technology, Pasadena, California 91125, United States
[3]Division of Engineering and Applied Science, California Institute of Technology, Pasadena, California 91125, United States
[4]Current Affiliation: National Center for Atmospheric Research, Boulder, Colorado, United States.
[5]Current Affiliation: Chemistry and Firearms Branch, US Army Criminal Investigation Laboratory, Forest Park, Georgia, United States
[6]Current Affiliation: Cooperative Institute for Research in Environmental Science and National Oceanic and Atmospheric Administration, Boulder, Colorado, United States.
[7]Current Affiliation: South Coast Air Quality Management District, Diamond Bar, California, United States
[8]Current Affiliation: Aerodyne Research, Billerica, Massachusetts, United States.

Correspondence to: Rebecca H. Schwantes (rschwant@caltech.edu, rschwant@ucar.edu)

Abstract. Hydroxyl radical (OH) oxidation of toluene produces the ring-retaining products cresol and benzaldehyde, and the ring-opening products bicyclic intermediate compounds and epoxides. Here, first- and later-generation OH oxidation products from cresol and benzaldehyde are identified in laboratory chamber experiments. For benzaldehyde, first-generation ring-retaining products are identified, but later-generation products are not detected. For cresol, low-volatility (saturation mass concentration, C^* ~3.5 x 10^4 - 7.7 x 10^{-3} μg m^{-3}) first- and later-generation ring-retaining products are identified. Subsequent OH addition to the aromatic ring of o-cresol leads to compounds such as hydroxy, dihydroxy, and trihydroxy methyl benzoquinones and dihydroxy, trihydroxy, tetrahydroxy, and pentahydroxy toluenes. These products are detected in the gas phase by chemical ionization mass spectrometry (CIMS) and in the particle phase using offline direct analysis in real time mass spectrometry (DART-MS). Our data suggest that the yield of trihydroxy toluene from dihydroxy toluene is substantial. While an exact yield cannot be reported as authentic standards are unavailable, we find that a yield for trihydroxy toluene from dihydroxy toluene of ~0.7 (equal to the reported yield of dihydroxy toluene from o-cresol (Olariu et al., 2002)) is consistent with experimental results for o-cresol oxidation under low-NO conditions. These results suggest that even though the cresol pathway accounts for only ~20% of the oxidation products of toluene, it is the source of a significant fraction (~20-40%) of toluene secondary organic aerosol (SOA) due to the formation of low-volatility products.

1 Introduction

Aromatic compounds are emitted from both anthropogenic (e.g., solvent use and motor vehicle exhaust) and natural (e.g., wildfires) processes. Oxidation of aromatic compounds leads to the formation of ozone (O_3) and secondary organic aerosol

(SOA) (Calvert et al., 2002, and references therein). Despite the number of studies performed, the spectrum of gas-phase aromatic oxidation products remains incomplete, especially those of later generation and those responsible for producing secondary organic aerosol. Toluene, one of the principal aromatic compounds present in the atmosphere, is emitted from both anthropogenic processes (∼60%) and biofuel/biomass burning (∼40%) (Henze et al., 2008). Chamber studies have measured

5 particularly high SOA mass yields (0.9-1.6 μg/μg) from toluene (Zhang et al., 2014) when correcting for vapor wall loss using the Statistical Oxidation Model. Modeling studies, using SOA yields that do not account for vapor wall loss (e.g., 0.1-0.3 μg/μg, (Ng et al., 2007)), estimated that toluene SOA contributes ∼4% of the total SOA produced globally (Henze et al., 2008). Incorporation of the updated SOA yields is expected to increase the calculated significance of toluene to the global SOA budget.

10 Hydroxyl radical (OH) oxidation of toluene takes place via four pathways, yielding benzaldehyde, cresol, bicyclic interme-diates, and epoxides (Figure 1). Identification of subsequent gas-phase oxidation products from the benzaldehyde and cresol pathways is the focus of this work. These ring-retaining compounds are likely to lead to SOA if the ring is retained during subsequent oxidation. Since OH addition to the aromatic ring of toluene increases the reaction rate constant for subsequent OH addition (Calvert et al., 2002), this chemistry accelerates the path to highly oxidized products.

15 Benzaldehyde forms as a result of hydrogen abstraction from the methyl group of toluene. Reported benzaldehyde yields from toluene oxidation are relatively consistent in the range of 0.053-0.12 (Calvert et al., 2002, and references therein). MCM v3.3.1 recommends a yield of 0.07, which is in the middle of this range (Jenkin et al., 2003; Bloss et al., 2005).

Cresol is produced from OH addition to the aromatic ring of toluene with subsequent O_2 addition and HO_2 elimination. Measured yields of cresol from toluene oxidation range from 0.03 to 0.385 (Calvert et al., 2002, and references therein) with

20 several studies converging to a yield of 0.18 (Klotz et al., 1998; Smith et al., 1998). A recent theoretical study suggests a cresol yield of 0.32 (Wu et al., 2014). Cresol yields from OH oxidation of toluene are difficult to measure quantitatively because cresol is prone to losses (e.g., to sampling tubing) that are dependent on the measurement technique (Klotz et al., 1998). Once formed, cresol (k_{OH} ∼5 x 10^{-11} cm^3 $molec^{-1}$ s^{-1}) reacts much faster with OH than its precursor toluene (k_{OH} = 6 x 10^{-12} cm^3 $molec^{-1}$ s^{-1}) (Calvert et al., 2002). Nakao et al. (2012) detected products in the particle phase indicative of successive

25 OH addition to the aromatic ring of o-cresol (i.e., $C_7H_8O_4$ and $C_7H_8O_5$) and phenol and estimated that the cresol pathway contributes ∼20% of SOA produced from toluene. Most studies (Olariu et al., 2002; Caralp et al., 1999) have focused on monitoring first-generation products from cresol and benzaldehyde in the gas-phase, but not second- and third- generation products. The goal of this work is to identify gas-phase pathways and specific oxidization products important for toluene SOA formation by monitoring later-generation products in the gas phase and linking these products to those detected in the particle

30 phase.

2 Methods

Chamber experiments were performed to study products from toluene OH oxidation under both low- and high-NO conditions. In order to explore later-generation chemistry and identify important precursors for SOA, later-generation ring-retaining products were also used as the initial precursor.

2.1 Experimental Design

All experiments were performed in the 24 m^3 Teflon chambers at the Caltech dual chamber facility. Low- and high-NO experiments were carried out in separate chambers to avoid contamination of NO and related compounds in the low-NO chamber. The chambers were flushed with purified air for 24 h prior to each experiment. Purified air is generated by removing volatile organic carbon, ozone, nitrogen oxides, and water vapor from compressed air. Experiments oxidizing toluene, o-cresol, 3-methyl catechol, and benzaldehyde under low- and high-NO conditions were performed (Table 1). For all experiments, hydrogen peroxide (H_2O_2) as an OH source was injected first by flowing purified air through a glass bulb heated to 36°C; 2 ppm of H_2O_2 was used for all gas-phase and high-NO particle-phase experiments, and 4 ppm H_2O_2 was used for low-NO particle-phase experiments.

After addition of the oxidant, the volatile organic compound (VOC) was injected. Toluene (99.8% purity) and benzaldehyde ($\geq$ 99% purity) were injected into a glass bulb using a gas-tight syringe. Purified air was passed into the glass bulb and subsequently injected into the chamber at 5 L min^{-1}. A weighed amount of o-cresol (99.5% purity) was heated to 49°C, and an excess amount of 3-methyl catechol (98% purity) was heated to 36°C while purified air was passed into a glass bulb. A water bath was used to provide consistent heating.

For high-NO experiments, NO (501 ppm in N_2, Scott Specialty Gases) was injected into the chamber using a calibrated mass flow controller at the start of the experiment, and continuously throughout the experiment. The goal of the continuous NO injection was to control the amount of NO present during the experiment, such that the level of NO_x remained as low as possible. A kinetic model is used to verify that these experimental conditions are relevant to the atmosphere (see Section 2.3).

For experiments in which particle-phase sampling was performed, the last step included atomization of 0.06 M ammonium sulfate through a ^{210}Po neutralizer and into the chamber. Photooxidation was initiated at least 1 h after all injections were complete to ensure adequate mixing. UV lights centered $\sim$350 nm are used in the Caltech chamber. The calculated photolysis rates for NO_2, H_2O_2, and NO_3 are 4.4 x 10^{-3}, 3.2 x 10^{-6}, and 2.3 x 10^{-3} s^{-1}, respectively. Because the UV lights emit only a low amount of visible light, NO_3 photolysis is low and uncertain in the chamber. NO_3 forms in the chamber and reacts rapidly with a number of compounds present, so lights remained on until all filters had been collected to ensure photolysis of NO_3 and more importantly continued generation of OH.

Some studies (Tan et al., 2009; Lim et al., 2010) have implicated glyoxal, an OH oxidation product of toluene, in SOA formation under humid conditions, and one study suggested that glyoxal leads to enhanced SOA growth by increasing OH concentrations rather than directly forming aerosol (Nakao et al., 2012). In the present study, all experiments were carried

out under dry conditions (RH < 10%) to simplify gas-phase measurements and to focus on the later-generation low-volatility products that form in the gas phase and partition to the particle phase.

In experiment 9, all procedures were the same as described in the proceeding paragraphs, but after 1.5 h of photooxidation, lights were turned off. While lights were off, the decay of 3-methyl catechol oxidation products due to wall deposition was
5 measured. In experiment 10, all procedures were the same as described above, but lights were turned on for only 3.2 h. Once an adequate level of oxidation products from 3-methyl catechol oxdiation was generated, the chamber experiment was ended and purified air was sampled by the CIMS to monitor the desorption of 3-methyl catechol oxidation products off the CIMS walls.

2.2 Chamber Instrumentation

Commercial instruments were used to monitor toluene, nitrogen oxides (NO_x), ozone (O_3), relative humidity (RH), and tem-
10 perature. Toluene was monitored by a gas chromatograph with a flame ionization detector (GC-FID, Agilent 6890N, HP-5 column). NO_x and O_3 were monitored by a Teledyne T2OO NO_x monitor and Horiba APOA-360 O_3 monitor, respectively. A Vaisala HMM211 probe was used to monitor temperature and RH. Gas-phase oxidized compounds were detected via a CF_3O^- Chemical Ionization Mass Spectrometer (CIMS) (Section 2.2.1). Particle-phase compounds were monitored using high-resolution direct analysis in real time mass spectrometry (DART-MS) from filters collected at the end of each experiment
15 (Section 2.2.2).

2.2.1 CIMS Description and Calibration

A chemical ionization mass spectrometer (CIMS) was used to monitor oxidized organic compounds in the gas-phase. The CIMS uses a custom-modified triple quadrupole mass analyzer (Varian 1200) (St. Clair et al., 2010). The instrument was operated in both negative and positive mode using CF_3O^- and $H_3O \cdot (H_2O)_n^+$, respectively, as the reagent ions. A compound
20 (A) with an affinity for fluorine interacts with CF_3O^- to form a complex (R1) or to fragment (e.g., R2-R5). The F^- transfer (R2), which occurs typically for acidic compounds, is the dominant fragmentation process. A compound is detected at its molecular weight + 85 for the complex ion and + 19 for the F^- transfer ion. In positive mode, H_3O^+ typically interacts with a compound along with $0 - n$ water molecules to form a complex ion at the molecular weight $+(18n + 1)$ (R6). Other ions (e.g., NO^+) also cluster in positive mode complicating interpretation of signals. The reactions are:

$$A + CF_3O^- \rightarrow CF_3O^- \cdot A \tag{R1}$$

$$A + CF_3O^- \rightarrow CF_2O + A_{(-H)}^- \cdot HF \tag{R2}$$

$$A + CF_3O^- + M \rightarrow CF_2O \cdot A_{-H}^- + HF + M \tag{R3}$$

$$A + CF_3O^- + M \rightarrow A^-_{-H} + CF_2O + HF + M \tag{R4}$$

$$A + CF_3O^- + M \rightarrow HF{\cdot}A^-_{-CO2} + CF_2O + CO_2 + M \tag{R5}$$

$$A + H^+{\cdot}nH_2O \rightarrow A \cdot H^+(H_2O)_n \quad n = 0, 1, 2, ... \tag{R6}$$
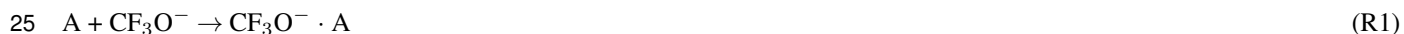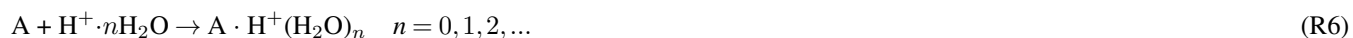
More detail about the ion chemistry of the CIMS is provided in St. Clair et al. (2010), Crounse et al. (2006), and Paulot et al.
(2009). Positive mode was used to monitor the decay of benzaldehyde, which is not detected in negative mode. Negative mode
was normalized by the total number of reagent ions. Signals were not normalized for positive mode, because the total reagent
ions (H_3O^+ and its water clusters) cannot be monitored.

MS/MS mode was used to confirm the identity of certain products and to separate isobaric compounds. In MS/MS mode,
only ions formed from the complex (R1) will produce a CF_3O^- daughter (m/z = (-)85). Ions formed from the F^- transfer
produce an $A^-_{(-H)}$ daughter (m/z = molecular weight of the analyte - 1). Detection of the $A^-_{(-H)}$ daughter and not the CF_3O^-
daughter confirms the ion forms from a F^- transfer and the analyte is acidic. The structural information provided by MS/MS
mode helps correctly identify compounds.

The CIMS was calibrated using o-cresol. An excess amount of o-cresol was heated at 46°C in a glass bulb. N_2 was blown
into this glass bulb and then directed into a Teflon pillow bag to produce a concentrated mixture containing ∼80 ppm of o-
cresol. A 500 mL glass bulb was filled from this concentrated bag. Fourier transform infrared absorption (FT-IR) spectroscopy
(pathlength 19 cm) was used to determine the concentration in the bulb. Part of the o-cresol sample in this bulb was lost in
order to fill the FT-IR cell, the rest was used to create a dilute pillow bag (∼200 ppb). The dilute pillow bag was filled with
either dry N_2 or the same purified air used to fill the large 24 m^3 Teflon chambers. This dilute pillow bag was then sampled by
the CIMS.

Independent of the calibrations described above, the loss of o-cresol to the glass FT-IR cell walls over time was measured by
filling the FT-IR cell with o-cresol and monitoring the decay. ∼8% was lost in the first 10 min and ∼24% after ∼1 h. Within
10 min of the FT-IR sample collection, the glass bulb was flushed into the dilute pillow bag. If wall deposition of o-cresol is
reversible, the o-cresol that deposited on the wall would be flushed into the pillow bag. Because the extent of reversibility of
o-cresol wall loss is unknown, a correction for wall loss was not applied, but instead added as uncertainty (8%). The o-cresol
integrated cross section for region 3145-2824 cm^{-1} measured by Etzkorn et al. (1999) was used for quantification. To our
knowledge there are no other reported FT-IR quantifications of o-cresol. In order to estimate the uncertainty in the o-cresol
quantification by Etzkorn et al. (1999), the m-cresol quantification from Etzkorn et al. (1999) (region 3178-2706 cm^{-1}) and
that from Pacific Northwest National Laboratory (PNNL) (Sharpe et al., 2004) were compared. The absorption spectra for
o-cresol and m-cresol in this region only partially align, but the integrated cross sections measured by Etzkorn et al. (1999)

are similar (12.7 x 10^{-18} and 12.6 x 10^{-18} cm molec^{-1}, respectively). The PNNL calibration (1 ppm) is 28% lower than the Etzkorn et al. (1999) calibration (1.39 ppm). The total uncertainty for the o-cresol sensitivity is then estimated as 36%, a combination of the uncertainty in the FT-IR quantification (28%) and loss of o-cresol during the calibration (8%).

As stated above, CF_3O^- interacts with an analyte (A) to form a complex (R1) or to fragment (e.g., R2-R5). o-Cresol predominantly forms a complex ion with CF_3O^- (Table 2). The distribution of the detected signals for each analyte is dependent on the stability of the molecular ion ($CF_3O^- \cdot A$). This stability is RH dependent (Table 2). Fragmentation to ions other than those described by R2-R5 is possible. These small ions cannot be used to determine the concentration of a compound because they are not uniquely formed from one compound. Instead the complex ion (R1) and all possible unique fragment ions (R2-R5) were considered in determining the concentration of a compound. Because the degree of fragmentation is dependent on the stability of the molecular ion, which is dependent on RH, the proportion of signals produced from R1-R5 needs to be known for all water levels used in the experiments. The influence of water on the distribution of o-cresol signals was determined by sampling a sustained amount of o-cresol and sequentially adding more water to the CIMS sampling inlet. The sum of all signals (i.e., complex ion (R1) and unique (R2-R5) and non-unique fragment ions) for o-cresol is stable over the range of relative humidities used in these experiments (Table 1). The CIMS sensitivity (including only unique signals (R1-R5)) determined from the FT-IR dry N_2 (RH <1%) calibration was corrected for the influence of water in the purified air (RH ~1-3%). This approach was within 10% of the FT-IR calibration, in which purified air was used to fill the dilute pillow bag instead of dry N_2. The water correction for o-cresol is minor. The CIMS sensitivity decreases by < 1% due to the slight RH increase over the course of the experiments.

3-methyl catechol calibration was attempted using the same FT-IR method as o-cresol. However, because the vapor pressure of 3-methyl catechol (6.8 x 10^{-6} atm) is much lower than that of o-cresol (3.9 x 10^{-4} atm) (Table 3), preparation of a sufficiently concentrated pillow bag for FT-IR quantification was not possible. Instead, the sensitivities of o-cresol and 3-methyl catechol were assumed to be the same in dry N_2 when including the sum of all detected signals (i.e., complex ion (R1) and unique (R2-R5) and non-unique fragment ions) with a correction for the difference in the ion-molecule collision rate between the compounds. The ion-molecule collision rate (dependent on the molecular weight, dipole moment, and polarizability of two colliding molecules) was estimated using the technique explained in Su and Chesnavich (1982) (see Section S1 and Tables S1 and S2 of the supplemental information for more details).

3-methyl catechol, which is more acidic than o-cresol, dominantly interacts with CF_3O^- to undergo an F^- transfer (R2, Table 2). Already a fragment, the F^- transfer ion is less stable than the complex ion and increasingly likely to decompose into smaller fragment ions as the mixing ratio of water increases (Table 2). The influence of water vapor on the sensitivity of 3-methyl catechol was measured in the same manner as that of o-cresol. Unlike o-cresol, the sum of all detected signals for 3-methyl catechol decreased as the relative humidity increased. Likely at higher water levels, more fragment ions formed below the detection limit (m/z = (-)50) of the CIMS. The sensitivity (including only unique signals (R1-R5)) decreased over the course of the experiments more for 3-methyl catechol (9-15%) than for o-cresol (<1%).

Because the CF_3O^- chemical ionization process for 3-methyl catechol exhibits more fragmentation and dependence on water than o-cresol, extrapolating the sensitivities to other more oxidized compounds (e.g., trihydroxy toluene) has a high degree

of uncertainty. The fragmentation and water dependence could exceed that for 3-methyl catechol. No authentic standards for trihydroxy toluene are currently available. However, two isomers (5-methyl-benzene-1,2,3-triol and 2,4,6-trihydroxytoluene) of trihydroxy toluene from Sigma's "collection of rare and unique chemicals" are available. Because Sigma does not validate the identity and purity of these compounds, these compounds were used only to examine the ion chemistry on the CIMS.

5 Purified air was flowed through a heated ($\sim$60-150°C) glass bulb containing each compound into a Teflon pillow bag. Due to the low volatility (saturation mass concentration, $C^* \sim 340 \ \mu g \ m^{-3}$) of these compounds, introducing detectable amounts into the gas phase without decomposition was extremely difficult.

2,4,6-trihydroxy toluene seemed to be more stable and a higher signal was achieved compared to 5-methyl-benzene-1,2,3-triol. Only major signals for 5-methyl-benzene-1,2,3-triol were above the noise and reported. For 2,4,6-trihydroxy toluene in

10 MS/MS mode, m/z (-)159 produced the m/z (-)139 daughter but not the m/z (-)115 daughter, and m/z (-)225 produced the m/z (-)205 daughter and only minor amounts of the m/z (-)85 daughter. In MS mode, 2,4,6-trihydroxy toluene produced the following signals m/z (-)225 $\sim$ 205 > 159 > 139 as well as many signals attributed to decomposition products or impurities (e.g., acetic acid). Although the signal intensity for 5-methyl-benzene-1,2,3-triol was low in MS/MS mode, which is less sensitive than MS mode, the signal intensity was sufficient to verify that m/z (-)159 produces the m/z (-)139 daughter. In MS

15 mode, 5-methyl-benzene-1,2,3-triol produced the following signals m/z (-)205 $\sim$ 159 > 225 > 139 and also produced a number of decomposition products or impurities (e.g., formic acid).

The CIMS detected many additional signals from these standards, which are likely caused by impurities, decomposition outside of the CIMS due to heating, and fragmentation inside the CIMS during chemical ionization. When the standards were introduced into the pillow bag at different temperatures, the ratio of these compounds to the m/z (-)159 (trihydroxy

20 toluene) signal was not consistent, suggesting these signals are largely due to impurities or decomposition outside of the CIMS. Fragmentation inside the CIMS during ionization would produce relatively consistent product fractions. Further understanding of the fragmentation occurring inside the instrument for trihydroxy toluene was unattainable owing to the high signals of impurities and decomposition products.

The sensitivity (all unique signals) determined for *o*-cresol was assumed to extend directly to the following compounds:

25 methyl hydroxy benzoquinone, methyl nitrophenol, benzoic acid, peroxy benzoic acid, phenyl hydroperoxide, nitrophenol, and dinitrophenol with a correction for the ion-molecule collision rate (Table S1). Similarly, the sensitivity (all unique signals) determined for 3-methyl catechol was assumed to extend directly to trihydroxy toluene, tetrahydroxy toluene, dihydroxy methyl benzoquinone, and dihydroxy nitrotoluene with a correction for the ion-molecule collision rate (Table S1). To the extent possible, all signals (complex, transfer, and potential unique fragmentation products (R1-R5)) for these compounds were used

30 to determine their mixing ratio.

During toluene oxidation, *m*-cresol and *p*-cresol also form. *o*-, *m*-, and *p*-cresol all produce similar amounts of non-unique fragmentation products in purified air (89-91%). Therefore, the slight difference in the ion-molecule collision rate (Table S1) and the isomer distribution produced during toluene oxidation (Klotz et al., 1998) was used to calculate a general cresol sensitivity.

2.2.2 DART-MS Description

SOA was collected during the final 4 h of experiments at 24 L min^{-1} on a Teflon membrane filter (47 mm, 1.0 μm pore size, Pall Life Sciences). The filters were analyzed by high-resolution direct analysis in real time mass spectrometry (DART-MS, JEOL, Inc.). A DART source is a low-temperature He plasma that generates primarily [A+H]$^{+}$ ions through proton transfer

5   reactions between the analyte, A, and ionized ambient water vapor (H$_3$O^{+}) (Cody et al., 2005; Cody, 2009). Samples are introduced directly into the DART stream, between the end of the DART source and the mass spectrometer inlet. A portion of the filter membrane was cut free from the support ring using a stainless steel scalpel and wrapped in a spiral around the barrel of a glass Pasteur pipet. The pipet was rotated slowly in the DART stream to warm the glass and desorb organic material gently from the Teflon filter. Each sample was cut and analyzed in triplicate. The final data are an average of these three replicates.

10   Additional analysis details and interpreted mass spectral data corrected to remove background ions are provided in Section S3 of the Supplemental Information.

With such a broad spectrum of compounds and the absence of synthetic standards, only ions with signals well above the background were selected for analysis. Ions with signals > 10% of the maximum ion signal (experiments 14 and 15) or second maximum ion signal (experiment 13) were selected. In experiment 13, the second maximum signal was used for peak selection

15   instead of the first because the first maximum ion signal dominated the mass spectrum (i.e., >6 times any other ion signal). The accurate m/z of each selected ion was assigned a chemical formula using ChemCalc (Patiny and Borel, 2013). This chemical formula was adjusted to its neutral form, and given a proposed structure based on the Master Chemical Mechanism (MCM) v3.3.1 (Jenkin et al., 2003; Bloss et al., 2005) toluene photooxidation mechanism, previously reported components of toluene SOA (Calvert et al., 2002; Olariu et al., 2002; Sato et al., 2007; Jang and Kamens, 2001; Nakao et al., 2011), and gas-phase

20   photooxidation products detected here by the CIMS.

DART-generated signal intensity for a given compound is proportional to the product of its vapor pressure, proton affinity, and concentration (Nilles et al., 2009; Schilling Fahnestock et al., 2015; Chan et al., 2013). Because the ion intensity is proportional to the vapor pressure, the vapor pressure of each compound needs to be known or estimated. Estimates of vapor pressures for low-volatility compounds have higher uncertainty due to lower availability and accuracy of experimental data

25   (Barley and McFiggans, 2010; O'Meara et al., 2014; Kurten et al., 2016). Thus, the results presented for the DART-MS analysis should be interpreted only qualitatively.

Two vapor pressure estimation methods are used here: 1) the Estimation of Vapor Pressure of Organics, Accounting for Temperature, Intramolecular, and Non-additivity Effects (EVAPORATION) method (Compernolle et al., 2011) and; 2) the method of Nannoolal et al. (2004, 2008). Both methods have online tools available for estimating the vapor pressure at http:

30   //tropo.aeronomie.be/models/evaporation_run.htm and http://www.aim.env.uea.ac.uk/aim/ddbst/pcalc_main.php, respectively. The EVAPORATION and Nannoolal methods are compatible with molecules containing oxygen-based functional groups and nitrates. Unlike the Nannoolal method, the EVAPORATION method has not been optimized for aromatic compounds, while the Nannoolal method cannot be used for diketones. Thus, EVAPORATION is used for all non-aromatic compounds and Nannoolal is used for all aromatics.

2.3 Kinetic Model

The chamber experiments were simulated with a kinetic model containing all reactions related to toluene from MCM v3.3.1 (Jenkin et al., 2003; Bloss et al., 2005), via http://mcm.leeds.ac.uk/MCM. Version 1 of the kinetic model includes all MCM v3.3.1 reactions relevant to toluene oxidation and inorganic chemistry, as well as experimentally measured wall deposition rates of o-cresol and dihydroxy toluene. Version 2 includes all reactions in Version 1 as well as photolysis of hydroxy nitrotoluene and dihydroxy nitrotoluene. Version 3 includes all reactions in Version 2 as well as additional oxidation reactions for dihydroxy toluene and benzaldehyde. Additional discussion of the kinetic model, including a list of reactions, is provided in Section S2 of the Supplemental information.

The kinetic model was used to evaluate the extent to which chamber conditions are representative of those in the atmosphere. The two main concerns in chamber studies performed under high-NO conditions are high NO_2 and NO_3 levels. Upon reaction with OH, a VOC forms an OH-VOC adduct, that will react with either NO_2 or O_2. Under atmospherically relevant conditions, the OH-VOC adduct reacts predominantly with O_2. The NO_2 reading on the NO_x monitor used in this study includes all NO_y products (e.g., organic nitrates, HNO_3, HONO, and NO_2). Instead of using the NO_x monitor, the kinetic model was used to predict the maximum NO_2 concentration. OH-o-cresol and OH-3-methyl catechol adducts are assumed to react at the same rate with NO_2 and O_2 as OH-m-cresol adduct (Koch et al., 2007), and the OH-benzaldehyde adduct was assumed to react with NO_2 and O_2 at the same rate as the OH-toluene adduct (Koch et al., 2007). The percent of OH-VOC adduct reacting with NO_2 versus O_2 for each experiment is presented in Table S5. For gas-phase experiments, the percentage of the OH-VOC adduct reacting with NO_2 was <6%. The higher loading necessary for the filter analysis required larger amounts of NO_x for the particle-phase experiments, for which the percentage of OH-VOC reacting with NO_2 was <10%.

Both o-cresol (1.4 x 10^{-11} cm^3 molec^{-1} s^{-1}, (Atkinson et al., 1992)) and 3-methyl catechol (1.7 x 10^{-10} cm^3 molec^{-1} s^{-1}, (Olariu et al., 2004)) react rapidly with NO_3. For the toluene high-NO experiments, a substantial amount of 3-methyl catechol and o-cresol is predicted to react with NO_3 (e.g., as much as 80% for the particle-phase experiments, Table S5). Caution is needed when interpreting results for high-NO oxidation conditions as both NO_3 and OH oxidation occur. In the present work, when starting with o-cresol or 3-methyl catechol, the percentage reacting with NO_3 was minor (e.g., < 4% for o-cresol for Experiment 5, Table S5). The kinetic model was also used to verify that RO_2 + RO_2 reactions were minimized for all experiments (Table S5). For example, in the toluene low-NO experiments, RO_2 + RO_2 reactions for the gas-phase and particle-phase experiments were estimated to be <12% and <18%, respectively, of all RO_2 pathways.

3 Results

Toluene reacts with OH to form both ring-retaining products (cresol and benzaldehyde) and ring-opening products (bicyclic intermediate compounds and epoxides) (Figure 1). Later generation gas-phase oxidation products from the ring-retaining pathways are identified. These oxidation products have a range of volatilities (C* ~5 x 10^5 - 7.7 x 10^{-3} μg m^{-3}). Compounds with the lower volatilities are detected in the particle phase, implying that the ring-retaining pathways are important for SOA formation. In order to monitor later generation products and constrain the pathways from which products emerge, oxidation

of first-generation products (*o*-cresol and benzaldehyde) and second-generation products (3-methyl catechol) was performed under both high- and low-NO conditions.

3.1   *o*-Cresol Oxidation

Previous studies generally recommend a ~0.18 yield of cresol (total of all isomers) from the toluene + OH pathway (Klotz et al., 1998; Smith et al., 1998) (Figure 1). The kinetic model (Version 1) assuming a 0.18 yield predicts cresol levels within the uncertainties of the CIMS measurements under both low- and high-NO conditions (Figure 2). As noted, version 1 of the kinetic model includes all MCM v3.3.1 reactions related to toluene and wall deposition (see Section 4.2.1) of *o*-cresol and dihydroxy toluene. An approximate cresol yield (~0.2) was calculated using the equation of Olariu et al. (2002) and the decay of toluene, rise in cresol, and accounting for losses of cresol from wall deposition and reaction with OH. The yield was calculated only under low-NO conditions. Under high-NO conditions, the correction for *o*-cresol reaction with NO_3 adds more uncertainty (Figure 2). The yield determined here is similar to that of other studies (Klotz et al., 1998; Smith et al., 1998).

The *o*-cresol oxidation mechanism in MCM v3.3.1, based on Olariu et al. (2002), is shown in black in Figure 3 for low-NO conditions and in Figure 4 for high-NO conditions. OH reacts with *o*-cresol via hydrogen abstraction to form a methyl phenoxy radical or addition to form either a bicyclic intermediate product or dihydroxy toluene. The reported dominant isomer of dihydroxy toluene is 3-methyl catechol (Olariu et al., 2002). Because the CIMS cannot explicitly separate different isomers, dihydroxy toluene is used throughout this work to represent all isomers. 3-methyl catechol is used when an explicit isomer is known (e.g., 3-methyl catechol was injected into the chamber). In experiment 4, in which 29 ppb of toluene was oxidized, the maximum detected mixing ratio of dihydroxy toluene was only ~0.2 ppb (Figure 2), emphasizing the importance of starting with later-generation products in order to determine the subsequent chemistry. Photooxidation of *o*-cresol produces dihydroxy toluene (m/z (-) 143) in agreement with Olariu et al. (2002). Under high-NO conditions, the methyl phenoxy radical reacts with NO_2 to form hydroxy nitrotoluene (m/z (-)172, F^- transfer and m/z (-)152, fragment).

3-Methyl catechol oxidation under both low- and high-NO conditions leads to the following products (Figure 3): trihydroxy toluene, hydroxy methyl benzoquinone, and various decomposition products presumably from the bicyclic intermediate pathway. These products likely result from OH addition to the ring of 3-methyl catechol. This pathway is not included in MCM v3.3.1, which assumes that hydrogen abstraction is the sole OH oxidation pathway for 3-methyl catechol. Dihydroxy nitrotoluene (m/z (-)188, F^- transfer and m/z (-)168, fragment), the expected product of hydrogen abstraction of 3-methyl catechol under high-NO conditions, is detected minimally (< 0.5 ppb) by the CIMS (Figures 4 and 10b & d). This suggests that hydrogen abstraction is not the dominant pathway for OH oxidation.

Without authentic standards for trihydroxy toluene and hydroxy methyl benzoquinone, quantification cannot be achieved (Section 2.2.1). Exact yields are not reported, but the experimental results are compared to the kinetic model (Section 4). Trihydroxy toluene is detected at several different signals in MS mode on the CF_3O^- CIMS: m/z (-)159 (F^- transfer), m/z (-)225 (complex), m/z (-)115 (fragment, possibly loss of CO_2), m/z (-) 205 (loss of HF from complex), and m/z (-) 139 (loss of HF from transfer). Three daughters are detected in MS/MS mode from m/z (-)159: m/z (-)139 (loss of HF), m/z (-)115 (possibly loss of CO_2), and m/z (-)85 (CF_3O^-). The presence of the m/z (-)85 daughter implies two compounds are detected at m/z (-

)159: trihydroxy toluene and another compound that forms a CF_3O^- complex (e.g., hydroxyacetone). Here MS/MS mode is used to separate the trihydroxy toluene signal from the interfering compound. Hydroxy methyl benzoquinone is detected at m/z (-)223 (complex), m/z (-)157 (F^- transfer), and m/z (-)137 (fragment).

Several products from photooxidation of trihydroxy toluene are also detected by the CIMS in the 3-methyl catechol oxidation experiments, including tetrahydroxy toluene, dihydroxy methyl benzoquinone, and various decomposition products from the bicylic intermediate pathway (Figure 3). Tetrahydroxy toluene, like trihydroxy toluene, is detected at m/z (-)175 (F^- transfer), m/z (-)241 (complex), and m/z (-)131 (fragment, possibly loss of CO_2). Dihydroxy methyl benzoquinone is detected at m/z (-)239 (complex), m/z (-)173 (F^- transfer), and m/z (-)153 (fragment). Trihydroxy methyl benzoquinone (m/z (-)189) and pentahydroxy toluene (m/z (-)191), likely oxidation products from tetrahydroxy toluene, are also detected by the CIMS, but the signals are close to background. As shown in Figure 3, OH oxidation of methyl benzoquinone possibly also forms products detected at the same mass as pentahydroxy toluene and dihydroxy methyl benzoquinone. However, these products are detected from 3-methyl catechol oxidation consistent with the proposed mechanism (Figure 3).

An array of decomposition products presumably from the bicyclic intermediate oxidation pathway of o-cresol, 3-methyl catechol, trihydroxy toluene, and tetrahydroxy toluene is detected (Figures 5 and 6). These decomposition products vary greatly in volatility (C* $\sim$ 2.2 x 10^6 to 14 μg m^{-3}). The highly oxygenated products such as $C_4H_4O_5$ and $C_5H_6O_5$ (C* $\sim$ 14 to 41 μg m^{-3}) are likely to result only from trihydroxy toluene and tetrahydroxy toluene oxidation, and are sufficiently low in volatility to partition in some degree to the particle phase. Because theoretical (PengZhen et al., 2012; Xu and Wang, 2013; Jorgensen, 2012) and experimental (Olariu et al., 2002) studies of OH addition to phenol and o-cresol all suggest $ortho$-addition is dominant, OH is presumed to also add to the $ortho$-position in Figures 5 and 6. OH addition to the other positions of the ring produces similar products. For o-cresol and 3-methyl catechol, all possibilities of OH addition are enumerated and the additional products appear at the bottom of Figure 5.

3.2   Benzaldehyde Oxidation

MCM v3.3.1 recommendations for OH oxidation of benzaldehyde are generally in agreement with the products detected by the CIMS (Figure 7). OH oxidation of benzaldehyde occurs via hydrogen abstraction of the formyl group followed by O_2 addition to form a peroxy radical. This peroxy radical reacts with HO_2 under low-NO conditions to form benzoic acid, peroxybenzoic acid, and phenyl hydroperoxide. Benzoic acid (m/z (-) 141) and peroxybenzoic acid (m/z (-)223) are the dominant first-generation products detected. Phenyl hydroperoxide (m/z (-)129) is minimally detected (<0.2 ppb) either due to a low yield or instability in the CIMS (Hydroperoxides have been known to fragment in the CF_3O^- CIMS (Praske et al., 2015)). As a result of the relatively large RO_2 + RO_2 rate constant for the peroxy radical of benzaldehyde (1.1 x 10^{-11} cm^3 $molec^{-1}$ s^{-1}), the benzaldehyde low-NO experiment was characterized by the kinetic model as having a higher fraction of RO_2 + RO_2 reactions than other experiments (Table S5). The proportions of benzoic acid and peroxybenzoic acid measured by the CIMS differ from those predicted by MCM v3.3.1 (see Section S1 and Figure S2 for more details).

Other first-generation products are also detected, including signals at m/z (-)155, (-)175, and (-)179. These minor signals comprise only 6%, 3%, and 5%, respectively, of the signals produced from benzoic and peroxybenzoic acids. Phenol is likely

at m/z (-)179. Compounds forming signals at m/z (-)155 and (-)175 rise with the other first-generation products, suggesting they are minor first-generation products from the $RO_2 + RO_2$ or $RO_2 + HO_2$ pathways.

The dominant first-generation product detected from benzaldehyde oxidation under high-NO conditions is nitrophenol (m/z (-)158, F^- transfer and m/z (-)138, fragment) (Figure 7). Dinitrophenol (m/z (-)203, F^- transfer and m/z (-)183, fragment), an OH oxidation product of nitrophenol, was also detected. Both products are over-predicted by MCM v3.3.1 using the kinetic model (Section 4.2.2 and Figure S3) compared to the CIMS measurements.

OH addition to the aromatic ring of benzaldehyde or benzoic acid is expected to be only a minor pathway. The rate of OH addition to an aromatic ring is proportional to the electrophilic nature of the substituents around the ring; unlike methyl and hydroxy groups, carboxy and formyl groups are not electrophilic (Calvert et al., 2002). OH addition to the ring of benzaldehyde would form hydroxy benzaldehyde, which is isobaric to benzoic acid. Only the transfer signal (m/z (-)141), not the complex (m/z (-)207), is detected, indicative that the product is highly acidic, like a carboxylic acid. Hydroxy benzoic acid is isobaric to peroxybenzoic acid, so the CIMS cannot explicitly confirm this product does not form. However, dihydroxy benzoic acid (m/z (-)173) as expected does not form.

Oxidation of benzaldehyde under high- and low-NO conditions does not yield many later generation products detectable by the CF_3O^- CIMS. The CIMS is expected to be sensitive to later generation products from the benzaldehyde pathway that retain the aromatic ring. Likely the main later generation products from benzaldehyde are ring-opening decomposition products, to which the CIMS is not sensitive (e.g., unfunctionalized ketones and aldehydes). Thus, we conclude that the cresol pathway is more important for SOA formation compared to the benzaldehyde pathway, based on the detectable products of the CF_3O^- CIMS and their expected volatilities (Table 3).

3.3 Products Detected in the Particle Phase by DART-MS

Products detected in the gas phase are compared to those detected in the particle phase to further understand the mechanism for toluene SOA formation. Filters, collected at the end of each experiment, were analyzed using high-resolution direct analysis in real time mass spectrometry (DART-MS). As expected, a number of compounds (e.g., trihydroxy toluene, tetrahydroxy toluene, and pentahydroxy toluene) measured in the gas-phase were also detected in the particle-phase by the DART-MS.

The intensity of the DART signal for a given compound is proportional to the product of the proton affinity, vapor pressure, and concentration of the compound. The proton affinity of each compound is assumed to be similar, due to shared ionizable functional groups. To compare the relative amounts of each product detected, the measured intensity is normalized by the compound's estimated vapor pressure to produce a normalized intensity (I_n). The relative fraction (R_f) of each compound is then calculated by dividing each compound's normalized intensity by the sum of the normalized intensities of all compounds in a given experiment. R_f values for each compound detected are reported in Tables S6-S8 in the Supplemental Information.

Vapor pressures for the compounds detected in this study have been estimated using both EVAPORATION and Nannoolal methods (Compernolle et al., 2011; Nannoolal et al., 2004, 2008). As noted earlier (Section 2.2.2), due to limitations in the methods, Nannoolal is used for all aromatics and EVAPORATION is used for all non-aromatic compounds. As demonstrated in Table 3, as the volatility of an aromatic compound decreases, the EVAPORATION method increasingly underestimates vapor

pressures as compared to Nannoolal. Owing to the uncertainty in these vapor pressure estimates, the reported R_f values should be considered only qualitatively.

The same o-cresol oxidation products, detected by the CIMS in the gas phase and expected to be low in volatility, are detected in the particle phase by the DART-MS. The corroborative analyses by CIMS and DART-MS support the proposed mechanism that OH subsequently adds to the ring of o-cresol forming low-volatility products. For example, the following are dominant products detected in the particle phase under low-NO oxidation of toluene (Figure 8a): polyols including trihydroxy toluene ($C_7H_8O_3$), tetrahydroxy toluene ($C_7H_8O_4$), and pentahydroxytoluene ($C_7H_8O_5$); benzoquinones including hydroxy methyl benzoquinone ($C_7H_6O_3$) and dihydroxy methyl benzoquinone ($C_7H_6O_4$); and various products from the bicyclic intermediate pathway including $C_4H_4O_2$, $C_5H_6O_2$, and $C_5H_6O_3$. Nakao et al. (2012) also detected $C_7H_8O_4$ and $C_7H_8O_5$ in the particle phase from o-cresol oxidation under low-NO conditions using a Particle-into-Liquid Sampler coupled with a Time-of-Flight Mass Spectrometer. Nakao et al. (2012) suspected these signals were due to successive OH addition to the aromatic ring; the combined CIMS and DART-MS analysis corroborates their conjecture.

As shown in Figure 8b, similar products were detected under toluene high-NO oxidation as toluene low-NO oxidation. Under high-NO conditions, methyl nitrophenol and dihydroxy nitrotoluene were also detected in the particle phase, albeit at lower relative fractions than many of the polyols and benzoquinone compounds (Figure 8b). At the end of the toluene high-NO experiment, estimated NO_3 oxidation of o-cresol (80%) and 3-methyl catechol (66%) was quite high compared to OH oxidation (Table S5). Part of the methyl nitrophenol signal could be influenced by NO_3 oxidation.

Some of the compounds (e.g., tetrahydroxy toluene and pentahydroxy toluene) are structural isomers of those produced from the epoxide pathway of toluene oxidation under low-NO conditions; under high-NO conditions, the products from the epoxide channel largely decompose (Figure S6). Signals assigned to tetrahydroxy toluene and pentahydroxy toluene are dominant in the particle phase from toluene oxidation under both high- and low-NO conditions (Figure 8). This is consistent with the products forming from the o-cresol oxidation mechanism proposed in Figure 3 rather than the epoxide mechanism. Hydroxy methyl hydroperoxy benzoquinone, a product of OH oxidation of methyl benzoquinone under low-NO conditions, and pentahydroxy toluene are structural isomers (Figure 3). Because the signal assigned to pentahydroxy toluene is detected under both low- and high-NO conditions, the product is more likely to be generated from tetrahydroxy toluene than methyl benzoquinone.

Nitrophenol from benzaldehyde oxidation is also detected in the particle phase. Part of the signal for $C_7H_6O_3$ may represent peroxybenzoic acid, as this compound is isobaric to hydroxy methyl benzoquinone. In general, products from cresol oxidation dominate over products from benzaldehyde oxidation in the particle phase. This is consistent with the gas-phase chemistry discussed in Section 3.2, in which few ring-retaining later generation products are detected from benzaldehyde oxidation.

3.4 Estimating the Contribution of Cresol to Toluene SOA

Considering that many products generated from the cresol pathway in the gas phase are also detected in the particle phase, the contribution of these products to toluene SOA is estimated. The experiments conducted here were optimized to investigate chemistry and not specifically designed to measure SOA yields, so this estimate is not based on the organic mass produced during each experiment. SOA yields studies are run differently to account for a variety of factors including particle and vapor

wall-losses. Chamber studies have recently reported toluene SOA mass yields to be between 0.9-1.6 $\mu g/\mu g$ when using the Statistical Oxidation Model to correct for vapor wall loss (Zhang et al., 2014). Without the model corrections for vapor wall loss, Zhang et al. (2014) measured the toluene SOA mass yields to be 0.5-0.65 $\mu g/\mu g$ for the experiments at maximum seed aerosol surface area (i.e., the experiments that most minimized vapor wall loss).

5   Under low-NO conditions the toluene SOA yield with the model corrections for vapor wall loss (1.6 $\mu g/\mu g$) implies a near unity carbon yield (Zhang et al., 2014), so at the lower bound the cresol pathway contributes to $\sim$20% of toluene SOA. For an upper bound estimate, we assume that trihydroxy toluene and hydroxy methyl benzoquinone and all oxidation products therefrom partition to the particle phase and that the average molecular weight of all compounds in the aerosol is equal to that of pentahydroxy toluene. With these assumptions and using the toluene SOA mass yield of 0.5 (the lowest yield explained above), the cresol pathway is estimated to contribute $\sim$40% of toluene SOA. Based on this, the contribution of the cresol pathway to toluene SOA is estimated as $\sim$20-40%.

4   Discussion

Gas- and particle-phase measurements by the CIMS and DART-MS confirm that OH oxidation of dihydroxy toluene leads to low-volatility products that partition to the particle phase. For example, the following three products, which form from subsequently adding OH to the aromatic ring, are detected in the gas and particle phases: trihydroxy toluene (C* $\sim$ 340 μg m^{-3}), tetrahydroxy toluene (C* $\sim$ 2.1 μg m^{-3}) and pentahydroxy toluene (C* $\sim$ 7.7 x 10^{-3} μg m^{-3}). Here, we discuss other theoretical and experimental work pertaining to OH addition to the aromatic ring and use the kinetic model to further interpret the CIMS results.

4.1   OH Addition to an Aromatic Ring

20 The chemical mechanism proposed in Figure 3 is consistent with previous observations of aromatic chemistry. As OH groups add to an aromatic ring, the aromatic ring becomes more activated, and the OH addition rate constant increases (Calvert et al., 2002). For example, the OH reaction rate constants for toluene, o-cresol, and 3-methyl catechol are 6 x 10^{-12}, 4 x 10^{-11}, and 2 x 10^{-10} cm^3 molec^{-1} s^{-1}, respectively (Calvert et al., 2002; Olariu et al., 2000).

     In the atmosphere, once OH adds to the aromatic ring, O$_2$ also adds, and one of the following five processes occurs: O$_2$ elimination, HO$_2$ elimination, bicyclic intermediate formation, intramolecular H-shift, or reaction with NO, HO$_2$ or RO$_2$ (Wu et al., 2014; Xu and Wang, 2013; Pan and Wang, 2014). For the toluene system, HO$_2$ elimination to re-form the aromatic ring or cyclization to form a bicyclic intermediate are the most commonly expected processes. Experiment and theory both suggest that HO$_2$ elimination occurs more rapidly than bicyclic intermediate formation for products with increasing OH substitution on the aromatic ring. Experimental studies report the cresol yield from toluene to be $\sim$0.2 (Klotz et al., 1998; Smith et al., 1998), while the 3-methyl catechol yield from o-cresol is $\sim$0.7 (Olariu et al., 2002). By analogy, the yield of trihydroxy toluene, the OH addition product from 3-methyl catechol, is also expected to be substantial. Theoretical calculations for phenol suggest that the elimination of HO$_2$ after O$_2$ addition occurs faster than the formation of a bicyclic intermediate (Xu and Wang, 2013). Xu

and Wang (2013) further suggest that the O_2 addition reaction rate constant for the phenol-OH adduct at 323 K (300 x 10^{-16} cm^3 $molec^{-1}$ s^{-1} (Koch et al., 2007)) is fast due to the rapid elimination of HO_2. In contrast, the O_2 addition rate constant for the toluene-OH adduct at 321K (5.6 x 10^{-16} cm^3 $molec^{-1}$ s^{-1} (Koch et al., 2007)) is much lower. Similarly, fast HO_2 elimination may enhance the O_2 addition rate constant in the cresol system as the O_2 addition rate constant for *m*-cresol-OH adduct (800 x 10^{-16} cm^3 $molec^{-1}$ s^{-1} (Zetzsch et al., 1997)) is even larger than that of phenol.

4.2 Comparing CIMS Measurements with Kinetic Model Predictions

In order to evaluate the products detected by the CIMS, the mechanism outlined in Figures 3-7 is incorporated into the kinetic model. Version 2 of the kinetic model includes photolysis of hydroxy nitrotoluene and dihydroxy nitrotoluene. Version 3 of the kinetic model includes additional products for 3-methyl catechol and benzaldehyde oxidation (see Section S2 for more details).

4.2.1 Vapor Wall Deposition

In order to compare the CIMS results to the kinetic model predictions, all loss processes need to be constrained for the compounds of interest. This includes reaction with OH/NO_3 and vapor wall deposition. Considering the reaction rate constant for 3-methyl catechol + OH is already fast (2.0 x 10^{-10} cm^3 $molec^{-1}$ s^{-1}) (Olariu et al., 2000), the hard sphere collision rate limit (2.5 x 10^{-10} cm^3 $molec^{-1}$ s^{-1}) is assumed for OH reaction with trihydroxy and tetrahydroxy toluene. The approximations for NO_3 oxidation are more speculative than those for OH oxidation, so more focus is given to comparing the CIMS measurements and the kinetic model results under low-NO conditions.

In experiment 9 (Table 1), lights were turned on to generate oxidation products of 3-methyl catechol. After 1.5 h, lights were turned off, and wall deposition rates of the following five compounds were measured: 3-methyl catechol, trihydroxy toluene, tetrahydroxy toluene, hydroxy methyl benzoquinone, and dihydroxy methyl benzoquinone. After 9 h of lights off at 28°C, the chamber was heated to 42°C for 4 h, then cooled to 16°C for 3 h, and finally heated back to 28°C for 3 h (Figure 9). An equilibrium is established for each compound between the gas phase and chamber wall. Heating and cooling the chamber disrupts this equilibrium. Most of the compounds did not significantly re-partition back into the gas phase when heating the chamber from 28°C to 42°C. This implies the absence of a large reversible reservoir on the chamber walls, so measuring the decay after 1.5 h of photooxidation is reasonable for these compounds. All of the compounds were lost to the walls faster at 16°C than at 28°C. As the chamber was heated from 16 to 28°C, some of the products slightly re-partitioned back to the gas phase, but not to the level expected if the chamber had not been cooled, suggesting that some loss was irreversible.

In experiment 10 (Table 1), photooxidation products from 3-methyl catechol were generated in the chamber. After 3.2 h of oxidation, purified air was sampled on the CIMS to monitor desorption of these oxidation products off the walls of the instrument. Desorption was minimal (i.e., within two scans, the signal was <0.08 of the original signal) for all of the five compounds measured except tetrahydroxy toluene (Figure S1). The signals for tetrahydroxy toluene dropped to ~1/2 their original value after sampling purified air, and slowly decayed from this point onward. Therefore, this compound is lost reversibly to the walls of the CIMS such that accurate quantification and wall loss determination is not possible. This was the

only compound that rose nearly to its original signal after heating the chamber to 42°C (Figure 9b, cyan), suggesting a possible large reversible reservoir of this compound on the wall as well.

For 3-methyl catechol (m/z (-)143), hydroxy methyl benzoquinone (m/z (-)157), and dihydroxy methyl benzoquinone (m/z 173), MS mode was used to determine the wall deposition rate constants (Figure 9b) (MS/MS mode produced similar results). The MS and MS/MS results for trihydroxy toluene (Figure 9a) imply that multiple isomers, with different wall loss rates and fragmentation patterns on the CIMS, are forming. For example, the wall loss rate determined from the MS signal m/z (-) 159 $(2.3 \times 10^{-5} \text{ s}^{-1})$ is different from those determined from the MS/MS daughters of m/z (-)159: $1.8 \times 10^{-5} \text{ s}^{-1}$ (m/z (-) 159), $1.9 \times 10^{-5} \text{ s}^{-1}$ (m/z (-)139), and $3.6 \times 10^{-5} \text{ s}^{-1}$ (m/z (-)115).

The pKa values of compounds similar to trihydroxy toluene demonstrate that aromatic compounds with an OH group *ortho* to another OH group are more acidic than those with an OH group *meta* or *para* to another OH group. For example, 1,2 dihydroxy benzene, 1,3 dihydroxy benzene, and 1,4 dihydroxy benzene have the following pKa values 9.36, 9.44, and 9.91, respectively (Dean, 1992). Likely the arrangement of the OH groups on trihydroxy toluene influences the acidity, which then influences both the wall deposition and the CIMS fragmentation patterns. The two standards of trihydroxy toluene monitored on the CIMS (Section 2.2.1) also demonstrate this effect. The isomer with the hydroxy groups spread out among the ring (2,4,6-trihydroxytoluene) was detected more at the complex than 5-methyl-benzene-1,2,3-triol, implying it is less acidic than 5-methyl-benzene-1,2,3-triol.

For simplicity, the wall deposition rate determined for m/z (-)159 is used in the kinetic model to represent the wall deposition of all trihydroxy toluene isomers, but in order to understand more fully the yield of this product, the isomer distribution and wall deposition for each isomer would need to be known. The water curve correction was applied in calculating the wall deposition rate constants for *o*-cresol, 3-methyl catechol, and trihydroxy toluene, but not for hydroxy methyl benzoquinone or dihydroxy methyl benzoquinone as the influence of water on benzoquinones is unknown. The *o*-cresol and 3-methyl catechol water curve corrections add 2×10^{-8} and $1.6 \times 10^{-6} \text{ s}^{-1}$ uncertainty, respectively, to the measured wall deposition rate constants. The wall deposition for tetrahydroxy toluene was approximated in the kinetic model since it cannot be measured. A plot of the natural log of C* versus the natural log of the wall deposition rate constant produces a fairly linear fit for the compounds measured in this work (Figure S5). This fit is used to approximate the wall loss of tetrahydroxy toluene, pentahydroxy toluene, and trihydroxy methyl benzoquinone. There is more uncertainty in the wall deposition rates for these compounds due to the necessity of extrapolation.

4.2.2 Formation and Loss of Nitro and Nitroso Compounds

MCM v3.3.1 does not include the photolysis of many nitro compounds, even though recent studies have measured fast photolysis rates (Bardini, 2006; Bejan et al., 2007, 2006). For example, hydroxy nitrotoluene has an atmospheric lifetime with respect to photolysis of < 1 h (Bejan et al., 2007). No studies thus far have reported the photolysis rate constants of dihydroxy nitrotoluene. In version 2 of the kinetic model, the photolysis rate constant for 6-methyl-2-nitrophenol (Bejan et al., 2007) was used for hydroxy nitrotoluene and dihydroxy nitrotoluene with a correction for the difference in the NO_2 photolysis rate constants between the Caltech chamber and that used by Bejan et al. (2007).

Under high-NO conditions during 3-methyl catechol oxidation, dihydroxy nitrotoluene is detected only minimally (< 0.5 ppb) even though the MCM v3.3.1 chemical mechanism predicts a peak value of $\sim$60 ppb (Figure 3 and Figure 10). Even after accounting for possible photolysis of dihydroxy nitrotoluene, the kinetic model (Version 2) still predicts a peak value of $\sim$45 ppb. Other nitro compounds are detected quite well by the CIMS (e.g., hydroxy nitrotoluene (Section 3.1) and nitrophenol (Section 3.2)), so this is unlikely caused by a sensitivity issue. Dihydroxy nitrotoluene has a lower estimated vapor pressure than the other nitro compounds detected (Table 3), so this compound is possibly lost to chamber walls and Teflon tubing to a higher degree. Considering the estimated photolyis rate constant (1.73×10^{-4} s^{-1}) is nearly an order of magnitude larger than the predicted wall deposition rate constant (1×10^{-5} s^{-1}, Figure S5), losses to chamber walls and Teflon tubing are unlikely the explanation for minimal detection of this compound. More likely, dihydroxy nitrotoluene, the expected product of hydrogen abstraction of 3-methyl catechol, is not, in fact, a main product. Contrary to the recommendations of MCM v3.3.1, hydrogen abstraction contributes only a small degree to OH oxidation of 3-methyl catechol.

MCM v3.3.1 predictions of nitrophenol, a product of benzaldehyde oxidation, exceed the CIMS measurements (Figure S3). An estimated photolysis rate constant was added to the kinetic model based on that for 2-nitrophenol measured by Bardini (2006) and reported by Chen et al. (2011). This photolysis rate constant was corrected for the difference in the photolysis of NO$_2$ between the Caltech chamber and the atmosphere when/where Bardini made the measurement. With this adjustment (Figure S3), nitrophenol is under-predicted by the kinetic model compared to the CIMS measurements, but within uncertainties in the CIMS sensitivity and the photolysis approximation.

4.2.3 *o*-Cresol Oxidation Products

During *o*-cresol oxidation, theory suggests that OH addition occurs dominantly *ipso* (position 2) or *ortho* (position 1 and 3) to the OH substituent due to hydrogen bonding (Jorgensen, 2012). Only OH addition to position 3 will form a dihydroxy toluene, as positions 1 and 2 do not have an abstractable hydrogen to undergo HO$_2$ elimination. Consistent with these theory calculations, Olariu et al. (2002) detected only 3-methyl catechol from *o*-cresol oxidation. Here, results suggest that 3-methyl catechol is not the only isomer of dihydroxy toluene that forms from *o*-cresol oxidation. 3-methyl catechol is detected mostly at the F$^-$ transfer ion (97%) and only minimally at the cluster ion (3%). However, dihydroxy toluene produced from *o*-cresol oxidation under low- and high-NO conditions is detected more at the complex ion ($\sim$12%) than 3-methyl catechol. This suggests that *o*-cresol oxidation produces an additional isomer or isomers. These isomer(s) are likely less acidic than 3-methyl catechol (i.e, the OH substituents are not on adjacent carbons). To verify this, dihydroxy toluene isomers were tested on the CF$_3$O$^-$ CIMS. 3-methyl catechol and 4-methyl catechol are dominantly detected at the F$^-$ transfer ion (m/z (-)143) (0.97 and 0.99, respectively) when considering only the unique signals (i.e., m/z (-)143, 123, 99, 209, and 189). Conversely, 2-methyl resorcinol and methyl hydroquinone signals are detected at m/z (-) 143, 189, and 209 at the following fractions 0.19, 0.51, & 0.30 and 0.07, 0.29, & 0.64, respectively. As expected, less acidic isomers of dihydroxy toluene (2-methyl resorcinol and methyl hydroquinone) were detected more at the complex ion (m/z = (-) 209) than their more acidic counterparts (3-methyl catechol and 4-methyl catechol).

In the kinetic model (Version 3), dihydroxy, trihydroxy, and tetrahydroxy toluene oxidation products are inferred from the products recommended by MCM v3.3.1 (Jenkin et al., 2003; Bloss et al., 2005) and Olariu et al. (2002) for o-cresol oxidation (Figure 3, Section S2). The hydrogen abstraction pathway is assumed to produce 6-methyl-2-nitrophenol and the bicyclic intermediate pathway is assumed to produce the unidentified products. Thus, dihydroxy, trihydroxy, and tetrahydroxy toluene are assumed to produce the following: a benzoquinone (0.07), a polyol (0.73), a product from the hydrogen abstraction pathway (0.07), and a product from the bicylic intermediate pathway (0.13). Isomers are not treated separately in the kinetic model. With these additional reactions, when oxidizing o-cresol under low-NO conditions, the kinetic model results are similar to the CIMS measurements for first-generation products (dihydroxy toluene) and second-generation products (hydroxy methyl benzoquinone and trihydroxy toluene) (Figure 10a). Although exact yields cannot be reported owing to the lack of availability of authentic standards, yields of ∼0.7 for trihydroxy toluene and ∼0.1 for hydroxy methyl benzoquinone from dihydroxy toluene oxidation appear to be reasonable. Additionally, the CIMS sensitivity (i.e., the ion-molecule collision rate correction, Section S1) for dihydroxy toluene and trihydroxy toluene is dependent on the isomers that form. The suspected dominant isomers of dihydroxy toluene (3-methyl catechol) and trihydroxy toluene (2,3,4-trihydroxy toluene) both have a higher sensitivity correction than their other isomer counterparts (Table S1). Thus, dihydroxy toluene and trihydroxytoluene may be underestimated by the CIMS if other isomers form to a large degree.

For 3-methyl catechol oxidation, like o-cresol oxidation, OH addition is assumed to occur at the *ortho* position forming 2,3,4-trihydroxy toluene as the dominant isomer. The wall deposition results (Section 4.2.1) imply that multiple isomers of trihydroxy toluene with different wall loss rates and fragmentation patterns on the CIMS are produced from 3-methyl catechol oxidation. Likely (as theory suggests), 2,3,4-trihydroxy toluene is the dominant isomer, but other isomers also form. Results suggest that the trihydroxy toluene isomers produced during o-cresol oxidation versus 3-methyl catechol oxidation are different. The distribution of the complex (m/z (-)225) , F$^-$ transfer (m/z (-)159), and fragment (m/z (-)115) signals for trihydroxy toluene is different during o-cresol oxidation (0.38, 0.42, 0.2, respectively) versus 3-methyl catechol oxidation (0.04, 0.42, 0.54, respectively). Likely the distribution of trihydroxy toluene isomers is different between the two cases because 3-methyl catechol is not the sole isomer of dihydroxy toluene produced from o-cresol oxidation. The isomers of trihydroxy toluene from o-cresol oxidation are detected more at the complex (likely less acidic), while the isomers from 3-methyl catechol oxidation fragment more (likely more acidic).

When 3-methyl catechol is oxidized under low-NO conditions, trihydroxy toluene is over-predicted by the kinetic model compared to the CIMS measurements (Figure 10c). Likely, the trihydroxy toluene isomers produced from 3-methyl catechol have a lower yield or CIMS sensitivity compared to those produced from o-cresol. In order to constrain the exact yield of trihydroxy toluene from dihydroxy toluene, the isomer distribution and wall deposition rate for each isomer need to be understood.

Under high-NO conditions, the kinetic model over-predicts trihydoxy toluene formation compared to the CIMS measurements for both o-cresol and 3-methyl catechol oxidation (Figure 10). Additionally, the kinetic model under-predicts methyl nitrophenol, a product from OH and NO_3 oxidation of o-cresol. This may indicate NO_3 loss due to photolysis is over-estimated in the kinetic model. Under-predicting the occurrence of NO_3 oxidation would lead to an over-prediction of OH oxidation products such as trihydroxy toluene and an under-prediction of NO_3 oxidation products such as methyl nitrophenol. The UV

lights (Section 2.1) used in the Caltech chamber emit only low levels of visible light such that the photolysis of NO_3 is difficult to quantify and does not sufficiently remove all NO_3.

Tetrahydroxy toluene and dihydroxy methyl benzoquinone are both over-predicted by the kinetic model under low- and high-NO conditions as compared to experimental results (Figure 10c & d). This low yield could be a result of unconstrained loses of tetrahydroxy toluene to the instrument walls or chamber walls. With the current instrumentation, further understanding of the yield of this product cannot be obtained.

4.2.4 Formation of Decomposition Products From Bicyclic Intermediate Pathway

OH addition to an aromatic ring followed by O_2 addition forms a peroxy radical. This peroxy radical can eliminate HO_2 forming products discussed in Section 4.2.3, eliminate O_2, cyclize and undergo O_2 addition to form a bicyclic intermediate peroxy radical (Atkinson et al., 1980), react with NO/HO_2, or undergo an intramolecular H-shift (Wu et al., 2014; Xu and Wang, 2013; Pan and Wang, 2014). Theoretical calculations suggest that the H-shift pathway and reaction with NO/HO_2 are negligible for phenol (Xu and Wang, 2013). Since compounds in this study are similar to phenol, the decomposition products detected are assumed to be produced from the bicyclic intermediate pathway.

In MCM v3.3.1, the bicyclic intermediate peroxy radical reacts either with NO producing an alkoxy radical that decomposes or with HO_2 producing a hydroperoxide. This hydroperoxide will either react with OH to reform the original RO_2 or photolyze to form decomposition products (Figure 3). Here, results suggest that either this hydroperoxide photolyzes more rapidly than MCM v3.3.1 assumes or the initial reaction with HO_2 proceeds through two reaction channels: 1) formation of a hydroperoxide and, 2) formation of OH and an alkoxy radical, which rapidly decomposes. Under low-NO conditions, the kinetic mechanism (Version 1) predicts most of the bicyclic intermediate products are in the form of the bicyclic intermediate hydroperoxide. Conversely, the CIMS measurements imply that most of the bicyclic intermediate products are in the form of decomposition products. o-Cresol and 3-methyl catechol oxidation under low- and high-NO conditions produce the same decomposition products rapidly and in high concentration. More specifically, for o-cresol oxidation under low-NO conditions, the CIMS detects acetyl acrylic acid, a decomposition product from the bicyclic intermediate pathway, at a peak of ∼1.5 ppb, while the kinetic mechanism predicts much less acetyl acrylic acid forms (peak ∼ 0.1 ppb). The CF_3O^- CIMS does not detect the bicyclic intermediate hydroperoxide. Either the signal is below the detection limit or the compound is not stable under CF_3O^- ion chemistry. Birdsall et al. (2010) similarly proposed that some of the bicyclic intermediate peroxy radical from toluene reacts with HO_2 to form an alkoxy radial and OH. Additionally, recent studies have identified various peroxy radicals that upon reaction with HO_2 do not form a hydroperoxide in unity yield (Orlando and Tyndall, 2012, and references therein). The additional OH produced from the bicyclic intermediate pathway would help explain why Version 3 of the kinetic model under-predicts the decay of the precursor (Figure 10).

A variety of decomposition products assumed to arise from the bicyclic intermediate pathway were detected by the CIMS (Figures 5 and 6). Largely, OH oxidation of o-cresol and 3-methyl catechol through the bicyclic intermediate pathway forms two product types: an unfuctionalized ketone/aldehyde, which is not detected by the CIMS, and a functionalized ketone/aldehyde, which is detected by the CIMS (Figure 5). For trihydroxy toluene and tetrahydroxy toluene often two functionalized ke-

tones/aldehydes form when the bicyclic ring fragments, so all products are detected by the CIMS. Many basic simplifications/assumptions are made to compare the CIMS and kinetic model results. All products are estimated to have the same CIMS sensitivity as glycolaldehyde. In the kinetic mechanism (version 3), o-cresol, 3-methyl catechol, trihydroxy toluene, and tetrahydroxy toluene are assumed to form a 0.13 yield of bicyclic intermediate products (Section 4.2.3). The OH reaction rate constant for all bicyclic intermediate compounds is assumed to be the same as that for acetyl acrylic acid (MCM v3.3.1).

With these additional reactions, the measurements of the bicyclic intermediate decomposition products formed from 3-methyl catechol oxidation under low- (Figure S4) and high-NO conditions are well represented by the kinetic model. These same products from o-cresol oxidation under low- and high-NO conditions, however, are under-predicted by the kinetic model (but still within uncertainty). Most of the products detected are not unique to one of the precursors (Figures 5 and 6). However, $C_4H_4O_5$ and $C_5H_6O_5$ are expected to form only from trihydroxy toluene and tetrahydroxy toluene. The CIMS measurements confirm $C_4H_4O_5$ and $C_5H_6O_5$ are produced later in the experiment, as expected for second- or third-generation products (Figure S4).

5 Atmospheric Relevance

The chemistry proposed (Figures 3 and 4), in which OH subsequently adds to the aromatic ring forming trihydroxy tolune, tetrahydroxy toluene, and pentahydroxy toluene, occurs under both low- and high-NO conditions. These low-volatility compounds are generated by OH addition to the aromatic ring with subsequent O_2 addition and HO_2 elimination. Because the peroxy radical formed during this process does not react with NO or HO_2, this pathway for forming SOA is not dependent on the traditional high-NO (RO_2 + NO) and low-NO (RO_2 + HO_2) definitions. Therefore, this work identifies a pathway for SOA formation that is relevant in both urban and rural regions. However, in urban areas heavily influenced by NO_x emissions NO_3 oxidation can be competitive with OH oxidation even during the day for compounds that react rapidly with NO_3 (Geyer et al., 2001, 2003; Khan et al., 2015; Brown et al., 2005; Kurtenbach et al., 2002). Large NO_3 reaction rate constants have been measured for many of the compounds produced from toluene OH oxidation (e.g., cresols and catechols) (Olariu et al., 2004; Atkinson et al., 1992). For example, during the day, $\sim$40% of p-cresol (Geyer et al., 2003) and 1,2 dihydroxy benzene (Olariu et al., 2004) are estimated to proceed via NO_3 rather than OH oxidation. The competition between NO_3 versus OH oxidation will depend on a variety of factors including the product of the NO_2 and O_3 concentrations and losses of NO_3 due to photolysis and reaction with NO. More modeling, field, and laboratory studies are needed to precisely constrain how cresol derived SOA is formed in the atmosphere especially under urban conditions. This work, by providing a better understanding of the gas- and particle-phase chemical mechanisms, can better define pathways that lead to different SOA yields and composition. For example, for cresol, competition between OH and NO_3 oxidation is more relevant than RO_2 fate. This knowledge can be used to correctly interpret chamber studies measuring SOA yields and parameterize SOA in global and regional chemical transport models.

Additionally, the proposed gas-phase chemical mechanism (Figures 3, 4, and 7) and composition of toluene derived SOA (Figure 8) together help identify toluene oxidation pathways that are most detrimental to human health. Several benzoquinone

type compounds (Figures 3 and 10) are detected in both the gas and particle phases. Quinones, which are potent oxidants and electrophiles, are well known to be toxic to humans (Monks et al., 1992, and references therein). Nitro aromatic compounds (Figures 4, 7, and 10) are also detected in the gas and particle phases. Nitro aromatic compounds are genotoxic and thereby also quite harmful to human health (Huang et al., 1995). Higher yields of nitro cresols have been measured from NO_3 oxidation (Olariu et al., 2013) than from OH oxidation (Olariu et al., 2002) implying the competition in urban air between NO_3 and OH oxidation is not only relevant for SOA yield, but also important for identifying potential health impacts. Benzaldehyde OH oxidation (Figure 7) produced a higher yield of nitro aromatics compared to cresol OH oxidation. Results from this study suggest that cresol due to the formation of low-volatility products plays a larger role in SOA formation than benzaldehyde. However, from a composition perspective, benzaldehyde OH oxidation due to higher yields of nitro and dinitro aromatics potentially has a higher impact on human health than cresol. Thus, the chemical mechanism and SOA composition described in this work can be combined with toxicology studies to better define how toluene oxidation impacts human health and air quality.

6 Conclusions

First- and later-generation cresol and benzaldehyde OH oxidation products are identified. Evidence suggests that later-generation products from cresol OH oxidation are particularly important for SOA formation. The following first-generation OH oxidation products of 3-methyl catechol (i.e., second-generation products from o-cresol) are detected: trihydroxy toluene, hydroxy methyl benzoquinone, and various decomposition products likely from the bicyclic intermediate pathway. Second- and third-generation products from 3-methyl catechol (i.e., third- and fourth-generation products from o-cresol) include tetrahydroxy toluene, dihydroxy methyl benzoquinone, pentahydroxy toluene, and trihydroxy methyl benzoquinone. Detection of these products implies that subsequent OH addition to the aromatic ring occurs during o-cresol oxidation. Many of these products are expected to be relatively low in volatility (C* $\sim$ 3.0 x 10^3 - 7.7 x 10^{-3} μg m^{-3}) and are detected in the particle phase by the DART-MS. Although the gas-phase cresol pathway is relatively minor ($\sim$20%), oxidation products from this pathway are estimated to contribute significantly ($\sim$20-40%) to toluene SOA. Thus, a simple and direct pathway for toluene SOA formation has been identified. Oxidation products from the phenolic pathway of other aromatic compounds are also likely to be important for SOA formation.

Acknowledgements. This work was supported by National Science Foundation grants AGS-1240604 and AGS-1523500. We thank Hannah Allen and Anke Noelscher for their experimental assistance and Nathan Dalleska and John Crounse for helpful discussions. The National Center for Atmospheric Research is sponsored by the National Science Foundation.

References

Atkinson, R., Carter, W. P. L., Darnall, K. R., and Winer, A. M. Pitts Jr., J. N.: A smog chamber and modeling study of the gas phase NO_x-air photooxidation of toluene and the cresols, Int. J. Chem. Kinet., 12, 779–836, 1980.

Atkinson, R., Aschmann, S. M., and Arey, J.: Reactions of OH and NO_3 radicals with phenol, cresols, and 2-nitrophenol at 296 ± 2 K, Environ. Sci. Technol., 26, 1397–1403, 1992.

Bardini, P.: Atmospheric chemistry of dimethylphenols and nitrophenols, Ph.D. Thesis, University College Cork, Thesis, 2006.

Barley, M. H. and McFiggans, G.: The critical assessment of vapour pressure estimation methods for use in modelling the formation of atmospheric organic aerosol, Atmos. Chem. Phys., 10, 749–767, 2010.

Bejan, I., Abd El Aal, Y., Barnes, I., Benter, T., Bohn, B., Wiesen, P., and Kleffmann, J.: The photolysis of *ortho*-nitrophenols: A new gas phase source of HONO, Phys. Chem. Chem. Phys., 8, 2028–2035, 2006.

Bejan, I., Barnes, I., Olariu, R., Zhou, S., Wiesen, P., and Benter, T.: Investigations on the gas-phase photolysis and OH radical kinetics of methyl-2-nitrophenols, Phys. Chem. Chem. Phys., 9, 5686–5692, 2007.

Birdsall, A. W., Andreoni, J. F., and Elrod, M. J.: Investigation of the role of bicyclic peroxy radicals in the oxidation mechanism of toluene, J. Phys. Chem. A., 114, 10 655–10 663, 2010.

Bloss, C., Wagner, V., Jenkin, M. E., Volkamer, R., Bloss, W. J., Lee, J. D., Heard, D. E., Wirtz, K., Martin-Reviejo, M., Rea, G., Wenger, J. C., and Pilling, M. J.: Development of a detailed chemical mechanism (MCMv3.1) for the atmospheric oxidation of aromatic hydrocarbons, Atmos. Chem. Phys., 5, 641–664, 2005.

Brown, S. S., Osthoff, H. D., Stark, H., Dube, W. P., Ryerson, T. B., Warneke, C., de Gouw, J. A., Wollny, A. G., Parrish, D. D., Fehsenfeld, F. C., and Ravishankara, A. R.: Aircraft observations of daytime NO_3 and N_2O_5 and their implications for tropospheric chemistry, J. Photochem. Photobiol. A, 176, 270–278, 2005.

Calvert, J., Atkinson, R., Becker, K. H., Kamens, R., Seinfeld, J., Wallington, T., and Yarwood, G.: The mechanisms of atmospheric oxidation of aromatic hydrocarbons, Oxford University Press, Inc., New York, 2002.

Caralp, F., Foucher, V., Lesclaux, R., Wallington, T. J., and Hurley, M. D.: Atmospheric chemistry of benzaldehyde: UV absorption spectrum and reaction kinetics and mechanisms of the $C_6H_5C(O)O_2$ radical, Phys. Chem. Chem. Phys., 1, 3509–3517, 1999.

Chan, M. N., Nah, T., and Wilson, K. R.: Real time in situ chemical characterization of sub-micron organic aerosols using direct analysis in real time mass spectrometry (DART-MS): The effect of aerosol size and volatility, Analyst, 138, 3749–3757, 2013.

Chen, J., Wenger, J. C., and Venables, D. S.: Near-ultraviolet absorption cross sections of nitrophenols and their potential influence on tropospheric oxidation capacity, J. Phys. Chem. A., 115, 12 235–12 242, 2011.

Cody, R. B.: Observation of molecular ions and analysis of nonpolar compounds with the direct analysis in real time ion source, Anal. Chem., 81, 1101–1107, 2009.

Cody, R. B., Laramee, J. A., and Durst, H. D.: Versatile new ion source for the analysis of materials in open air under ambient conditions, Anal. Chem., 77, 2297–2302, 2005.

Compernolle, S., Ceulemans, K., and Muller, J. F.: EVAPORATION: A new vapour pressure estimation method for organic molecules including non-additivity and intramolecular interactions, Atmos. Chem. Phys., 11, 9431–9450, 2011.

Crounse, J. D., McKinney, K. A., Kwan, A. J., and Wennberg, P. O.: Measurement of gas-phase hydroperoxides by chemical ionization mass spectrometry, Anal. Chem., 78, 6726–6732, http://pubs.acs.org/doi/abs/10.1021/ac0604235, 2006.

Dean, J. A.: Lange's handbook of chemistry 14th Ed., McGraw-Hill, Inc., New York, 1992.

Etzkorn, T., Klotz, B., Sorensen, S., Patroescu, I. V., Barnes, I., Becker, K. H., and Platt, U.: Gas-phase absorption cross sections of 24 monocyclic aromatic hydrocarbons in the UV and IR spectral ranges, Atmos. Environ., 33, 525–540, 1999.

Geyer, A., Alicke, B., Konrad, S., Schmitz, T., Stutz, J., and Platt, U.: Chemistry and oxidation capacity of the nitrate radical in the continental boundary layer near Berlin, J. Geophys. Reas., 106, 8013–8025, 2001.

5 Geyer, A., Alicke, B., Ackermann, R., Martinez, M., Harder, H., Brune, W., di Carlo, P., Williams, E., Jobson, T., Hall, S., Shetter, R., and Stutz, J.: Direct observations of daytime NO_3: Implications for urban boundary layer chemistry, J. Geophys. Reas., 108, 2003.

Henze, D. K., Seinfeld, J. H., Ng, N. L., Kroll, J. H., Fu, T. M., Jacob, D. J., and Heald, C. L.: Global modeling of secondary organic aerosol formation from aromatic hydrocarbons: high- vs. low-yield pathways, Atmos. Chem. Phys., 8, 2405–2421, 2008.

Huang, Q., Wang, L., and Han, S.: The genotoxicity of substituted nitrobenzenes and the quantitative structure-activity relationship studies,
10 Chemosphere, 30, 915–923, 1995.

Jang, M. and Kamens, R. M.: Characterization of secondary aerosol from the photooxiation of toluene in the presense of NO_x and 1-propene, Environ. Sci. Technol., 35, 3626–3639, 2001.

Jenkin, M. E., Saunders, S. M., Wagner, V., and Pilling, M. J.: Protocol for the development of the Master Chemical Mechanism, MCM v3 (Part B): tropospheric degradation of aromatic volatile organic compounds, Atmos. Chem. Phys., 3, 181–193, 2003.

15 Jorgensen, S.: Gas-phase oxidation of cresol isomers initiated by OH or NO_3 radicals in the presence of NO_2, Int. J. Chem. Kinet., 44, 165–178, 2012.

Khan, M. A. H., Morris, W. C., Watson, L. A., Galloway, M., Hamer, P. D., Shallcross, B. M. A., Percival, C. J., and Shallcross, D. E.: Estimation of daytime NO_3 radical levels in the UK urban atmosphere using the steady state approximation method, Advances in Meteorology, 2015, 2015.

20 Klotz, B., Sorensen, S., Barnes, I., Becker, K. H., Etzkorn, T., Volkamer, R., Platt, U., Wirtz, K., and Martin-Reviejo, M.: Atmospheric oxidation of toluene in a large-volume outdoor photoreactor: in situ determination of ring-retaining product yields, J. Phys. Chem. A., 102, 1998.

Koch, R., Knispel, R., Elend, M., Siese, M., and Zetzsch, C.: Consecutive reactions of aromatic-OH adducts with NO, NO_2 and O_2: benzene, naphthalene, toluene, *m*- and *p*-xylene, hexamethylbenzene, phenol, *m*-cresol and aniline, Atmos. Chem. Phys., 7, 2057–2071, 2007.

25 Kurten, T., Tiusanen, K., Roldin, P., Rissanen, M., Luy, J.-N., Boy, M., Ehn, M., and Donahue, N.: α-Pinene autoxidation products may not have extremely low saturation vapor pressures despite high O:C ratios, J. Phys. Chem. A., 120, 2569–2582, 2016.

Kurtenbach, R., Ackermann, R., Becker, K. H., Geyer, A., Gomes, A. G., Lorzer, J. C., Platt, U., and Wiesen, P.: Verification of the contribution of vehicular traffic to the total NMVOC emissions in Germany and the importance of the NO_3 chemistry in the city air, J. Atmos. Chem., 42, 395–411, 2002.

30 Lim, Y. B., Tan, Y., Perri, M., Seitzinger, S. P., and Turpin, B. J.: Aqueous chemistry and its role in secondary organic aerosol (SOA) formation, Atmos. Chem. Phys., 10, 10 521–10 539, 2010.

Monks, T. J., Hanzlik, R. P., Cohen, G. M., Ross, D., and Graham, D. G.: Quinone chemistry and toxicity, Toxicol. Appl. Pharmacol., 112, 2–16, 1992.

Nakao, S., Clark, C., Tang, P., Sato, K., and Cocker, D. I.: Secondary organic aerosol formation from phenolic compounds in the absence of
35 NO_x, Atmos. Chem. Phys., 11, 10 649–10 660, 2011.

Nakao, S., Liu, Y., Tang, P., Chen, C.-L., Zhang, J., and Cocker III, D. R.: Chamber studies of SOA formation from aromatic hydrocarbons: observation of limited glyoxal uptake, Atmos. Chem. Phys., 12, 3927–3937, 2012.

Nannoolal, Y., Rarey, J., Ramjugernath, D., and Cordes, W.: Estimation of pure component properties part 1. Estimation of the normal boiling point of non-electrolyte organic compounds via group contributions and group interactions, Fluid Phase Equilibria, 226, 45–63, 2004.

Nannoolal, Y., Rarey, J., and Ramjugernath, D.: Estimation of pure component properties part 3. Estimation of the vapor pressure of non-electrolyte organic compounds via group contributions and group interactions, Fluid Phase Equilibria, 269, 117–133, 2008.

5 Ng, N. L., Kroll, J. H., Chan, A. W. H., Chhabra, P. S., Flagan, R. C., and Seinfeld, J. H.: Secondary organic aerosol formation from *m*-Xylene, toluene, and benzene, Atmos. Chem. Phys., 7, 3909–3922, 2007.

Nilles, J. M., Connell, T. R., and Durst, H. D.: Quantitation of chemical warfare agents using the direct analysis in real time (DART) technique, Anal. Chem., 81, 6744–6749, 2009.

Olariu, R. I., Barnes, I., Becker, K. H., and Klotz, B.: Rate coefficients for the gas-phase reaction of OH radicals with selected dihydroxy-

10 benzenes and benzoquinones, Int. J. Chem. Kinet., 32, 696–702, 2000.

Olariu, R. I., Klotz, B., Barnes, I., Becker, K. H., and Mocanu, R.: FT–IR study of the ring-retaining products from the reaction of OH radicals with phenol, *o*-, *m*-, and *p*-cresol, Atmos. Environ., 36, 3685–3697, 2002.

Olariu, R. I., Bejan, I., Barnes, I., Klotz, B., Becker, K. H., and Wirtz, K.: Rate Coefficients for the Gas-Phase Reaction of NO_3 Radicals with Selected Dihydroxybenzenes, Int. J. Chem. Kinet., 36, 577–583, 2004.

15 Olariu, R. I., Barnes, I., Bejan, I., Arsene, C., Vione, D., Klotz, B., and Becker, K. H.: FT-IR product study of the reactions of NO_3 radicals With *ortho*-, *meta*-, and *para*-cresol, Environ. Sci. Technol., 47, 7729–7738, 2013.

O'Meara, S., Booth, A. M., Barley, M. H., Topping, D., and McFiggans, G.: An assessment of vapour pressure estimation methods, Phys. Chem. Chem. Phys., 16, 19 453–19 469, 2014.

Orlando, J. J. and Tyndall, G. S.: Laboratory studies of organic peroxy radical chemistry: an overview with emphasis on recent issues of

20 atmospheric significance, Chem. Soc. Rev., 41, 6294–317, doi:10.1039/c2cs35166h, http://www.ncbi.nlm.nih.gov/pubmed/22847633http://pubs.rsc.org/en/Content/ArticleLanding/2012/CS/c2cs35166h, 2012.

Pan, S. and Wang, L.: Atmospheric oxidation mechanism of m-xylene initiated by OH radical, J. Phys. Chem. A., 118, 10 778–10 787, 2014.

Patiny, L. and Borel, A.: ChemCalc: a building block for tomorrow's chemical infrastructure, J. Chem. Inf. Model., 53, 1223–1228, 2013.

Paulot, F., Crounse, J. D., Kjaergaard, H. G., Kroll, J. H., Seinfeld, J. H., and Wennberg, P. O.: Isoprene photooxidation: new insights into

25 the production of acids and organic nitrates, Atmos. Chem. Phys., 9, 1479–1501, 2009.

PengZhen, W. U., Jian, L. I., ShuJin, L. I., and Fu-Ming, T. A. O.: Theoretical study of mechanism and kinetics for the addition of hydroxyl radical to phenol, Sci China Chem, 55, 270–276, 2012.

Praske, E., Crounse, J. D., Bates, K. H., Kurten, T., Kjaergaard, H. G., and Wennberg, P. O.: Atmospheric fate of methyl vinyl ketone: peroxy radical reactions with NO and HO_2, J. Phys. Chem. A., 119, 4562–4572, 2015.

30 Sato, K., Hatakeyama, S., and Imamura, T.: Secondary organic aerosol formation during the photooxidation of toluene: NO_x dependence of chemical composition, J. Phys. Chem. A., 111, 9796–9808, 2007.

Schilling Fahnestock, K. A., Yee, L. D., Loza, C. L., Coggon, M. M., Schwantes, R. H., Zhang, X., Dalleska, N. F., and Seinfeld, J. H.: Secondary organic aerosol composition from C_{12} alkanes, J. Phys. Chem. A., 119, 4281–4297, 2015.

Sharpe, S. W., Johnson, T. J., Sams, R. L., Chu, P. M., Rhoderick, G. C., and Johnson, P. A.: Gas-phase databases for quantitative infrared

35 spectroscopy, composite spectrum for MCRESOL_25T, Version 1.0, July, 03, Applied Spectroscopy, 58, 1452–1461, 2004.

Smith, D. F., McIver, C. D., and Kleindienst, T. E.: Primary product distribution from the reaction of hydroxyl radicals with toluene at ppb NO_X mixing ratios, J. Atmos. Chem., 30, 209–228, 1998.

St. Clair, J. M., McCabe, D. C., Crounse, J. D., Steiner, U., and Wennberg, P. O.: Chemical ionization tandem mass spectrometer for the in situ measurement of methyl hydrogen peroxide, Rev. Sci. Instrum., 81, 094 102–094 102, doi:10.1063/1.3480552, http://www.ncbi.nlm.nih.gov/pubmed/20886995, 2010.

Su, T. and Chesnavich, W. J.: Parametrization of the ion-polar molecule collision rate constant by trajectory calculations, J. Chem. Phys., 76, 5183–5185, 1982.

Tan, Y., Perri, M. J., Seitzinger, S. P., and Turpin, B. J.: Effects of precursor concentration and acidic sulfate in aqueous glyoxal-OH radical oxidation and implications for secondary organic aerosol, Environ. Sci. Technol., 43, 8105–8112, 2009.

Wu, R., Pan, S., Li, Y., and Wang, L.: Atmospheric oxidation mechanism of toluene, J. Phys. Chem. A., 118, 4533–4547, 2014.

Xu, C. and Wang, L.: Atmospheric oxidation mechanism of phenol initiated by OH radical, J. Phys. Chem. A., 117, 2358–2364, 2013.

Yaws, C. L.: Handbook of vapor pressures: C_5 to C_7 compounds, vol. 2, Gulf Publishing Company, Houston, Texas, 1994.

Zetzsch, C., Koch, R., Bohn, B., Knipsel, R., Siese, M., and Witte, F.: Adduct formation of OH with aromatics and unsaturated hydrocarbons and consecutive reactions with O_2 and NO_x to regenerate OH, in: Chemical Processes in Atmospheric Oxidation, edited by LeBras, G., pp. 247–256, Springer-Verlag, Berlin, 1997.

Zhang, X., Cappa, C. D., Jather, S. H., McVay, R. C., Ensberg, J. J., Kleeman, M. J., and Seinfeld, J. H.: Influence of vapor wall loss in laboratory chambers on yields of secondary organic aerosol, P. Natl. Acad. Sci. USA, 111, 5802–5807, 2014.
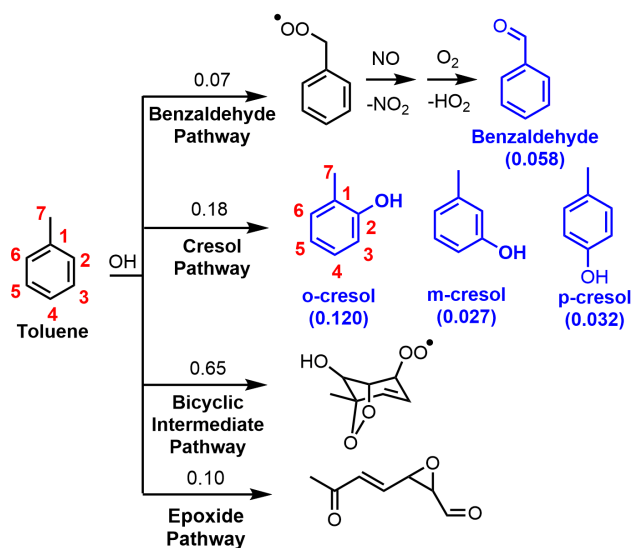
Figure 1. Toluene photooxidation pathways from the Master Chemical Mechanism (MCM) v3.3.1 including cresol isomer distribution (Klotz et al., 1998). Ring-retaining products are shown in blue. Carbons on the toluene and *o*-cresol ring structure are labeled in red from 1-7 to facilitate identification of isomers throughout the text.
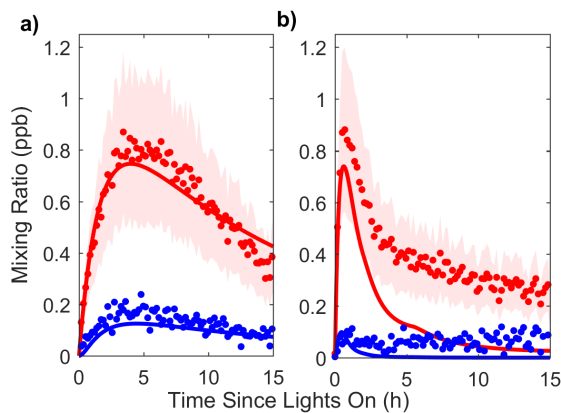
Figure 2. Kinetic model predictions (Version 1 solid lines) compared to CIMS measurements (data points) under low-NO (a, experiment 4) and high-NO (b, experiment 3) oxidation of toluene for cresol (red) and dihydroxy toluene (blue). The uncertainty in the CIMS measurements for cresol is shown in red shading. The CIMS measurements under high-NO conditions (panel b) suggest that additional first- or second-generation products that react much slower with OH than cresol give rise to signal at the same mass.
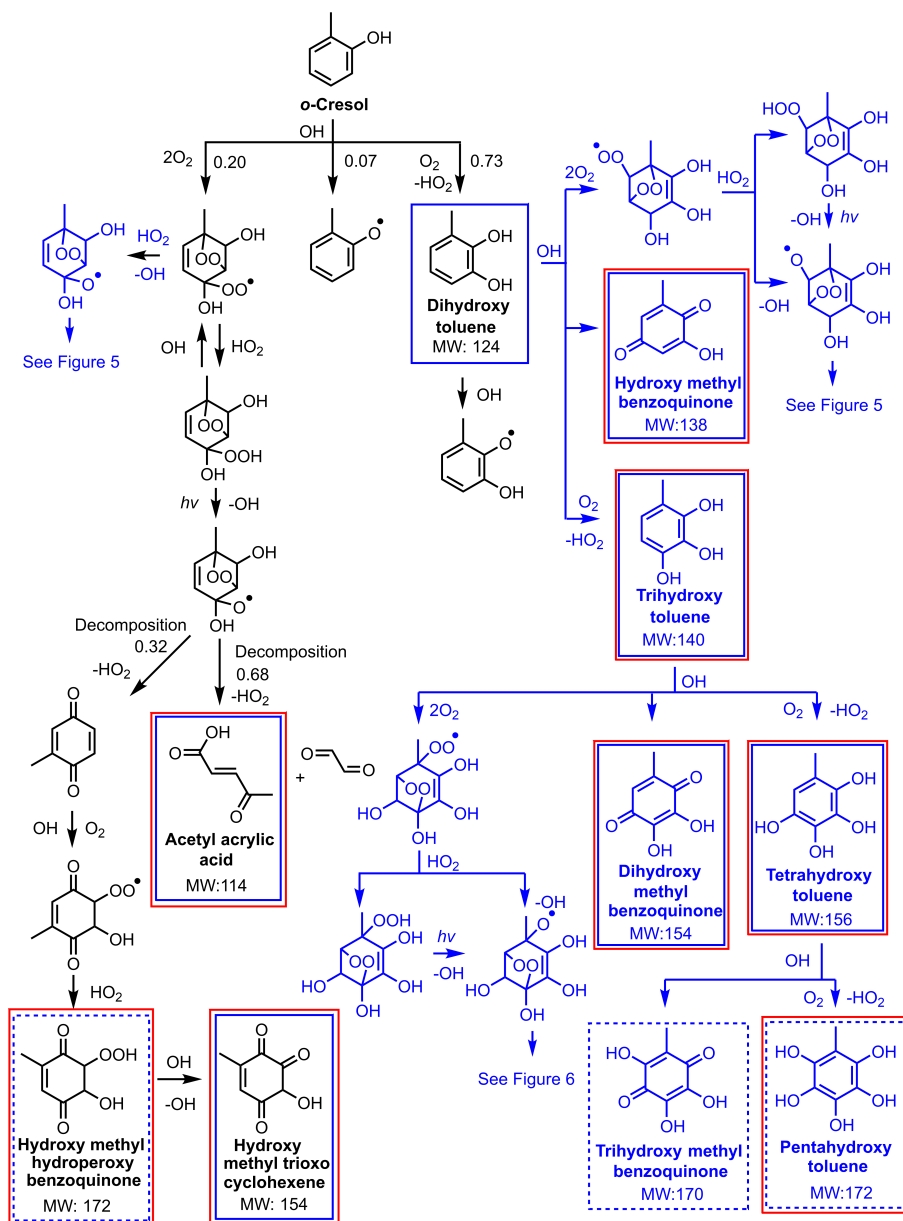
Figure 3. Gas-phase chemical mechanism for *o*-cresol photooxidation under low-NO conditions. Recommended pathways by MCM v3.3.1 are shown in black. The proposed mechanism from the present study is shown in blue. Products detected in this study by the CIMS and DART-MS are outlined in blue and red boxes, respectively, with dashed lines indicating compounds detected at only a minimal level. The reported dominant isomer of dihydroxy toluene, 3-methyl catechol, is shown (Olariu et al., 2002).
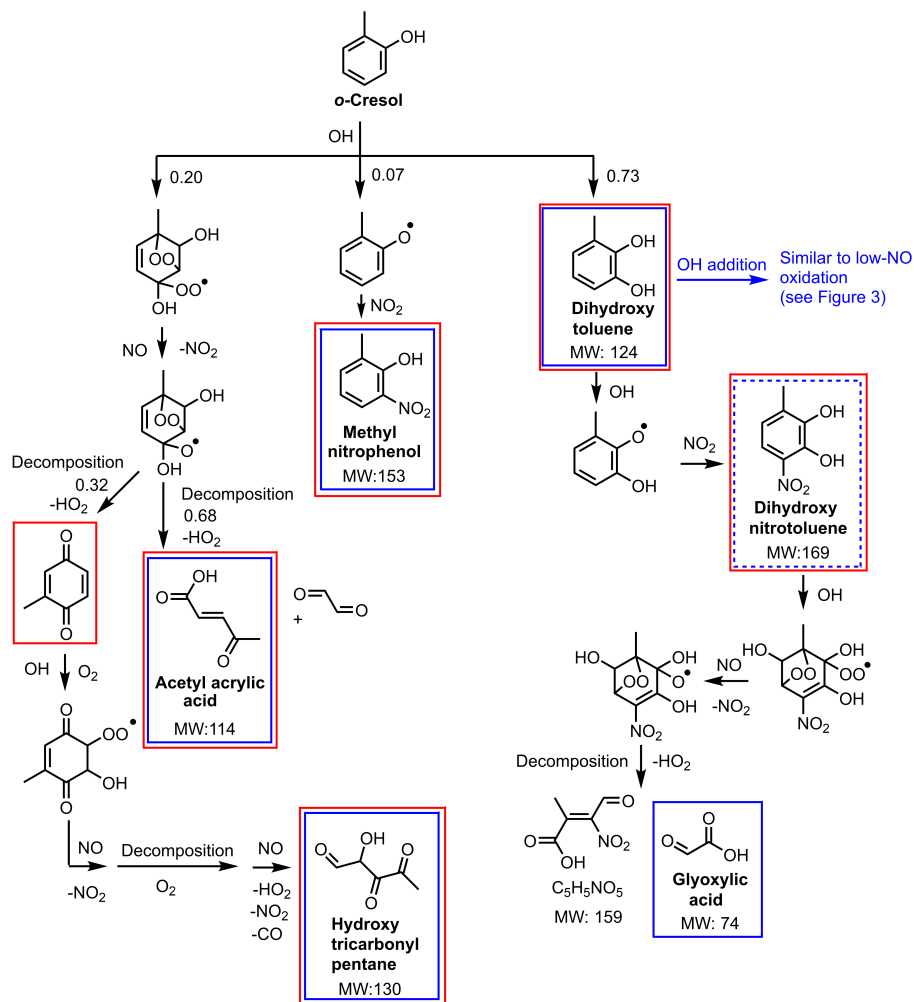
Figure 4. Gas-phase chemical mechanism for *o*-cresol photooxidation under high-NO conditions. The MCM v3.3.1 scheme is shown in black. Products outlined in blue were detected in the present study by the CIMS with dashed lines indicating only a minor amount was detected. Red boxed compounds were detected in the present study by the DART-MS. OH addition to dihydroxy toluene forms similar products as the low-NO system (see Figure 3).
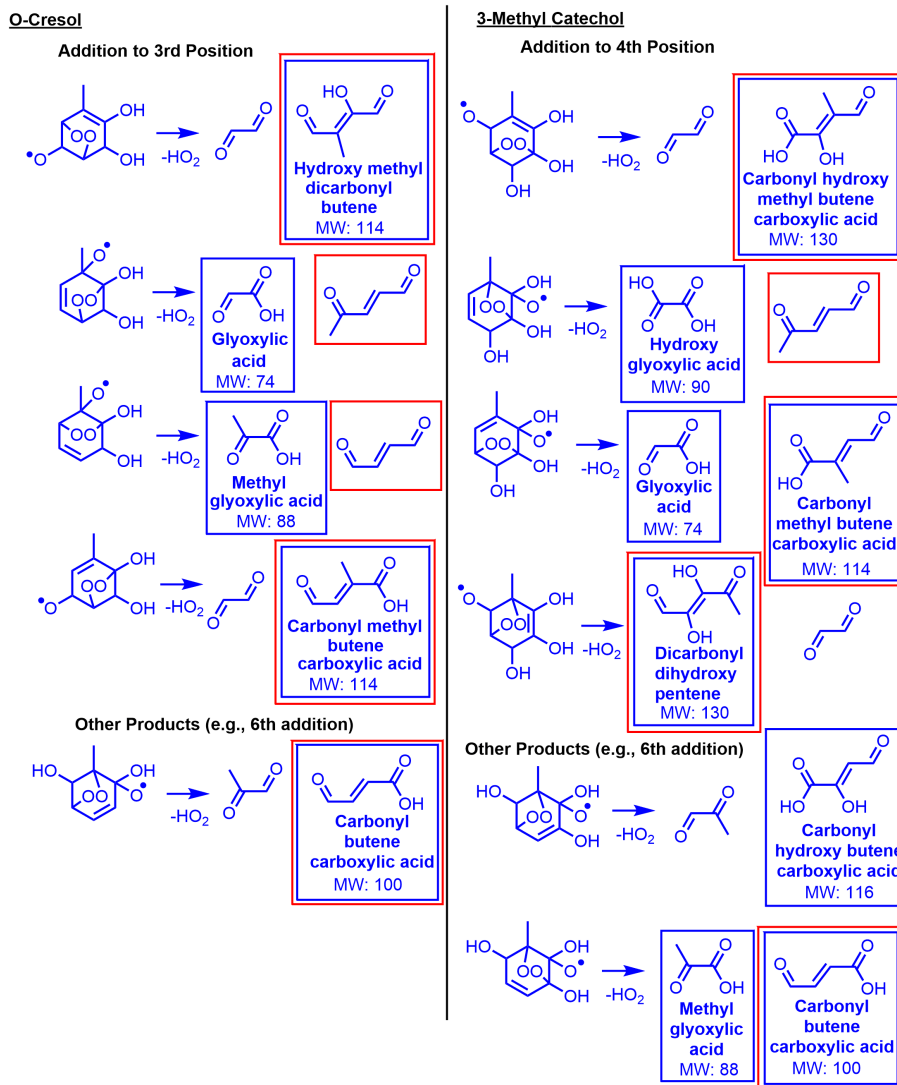
Figure 5. Proposed decomposition pathways for bicyclic intermediate compounds formed from OH oxidation of *o*-cresol and 3-methyl catechol. Blue and red boxed compounds were detected by CIMS and DART-MS, respectively.
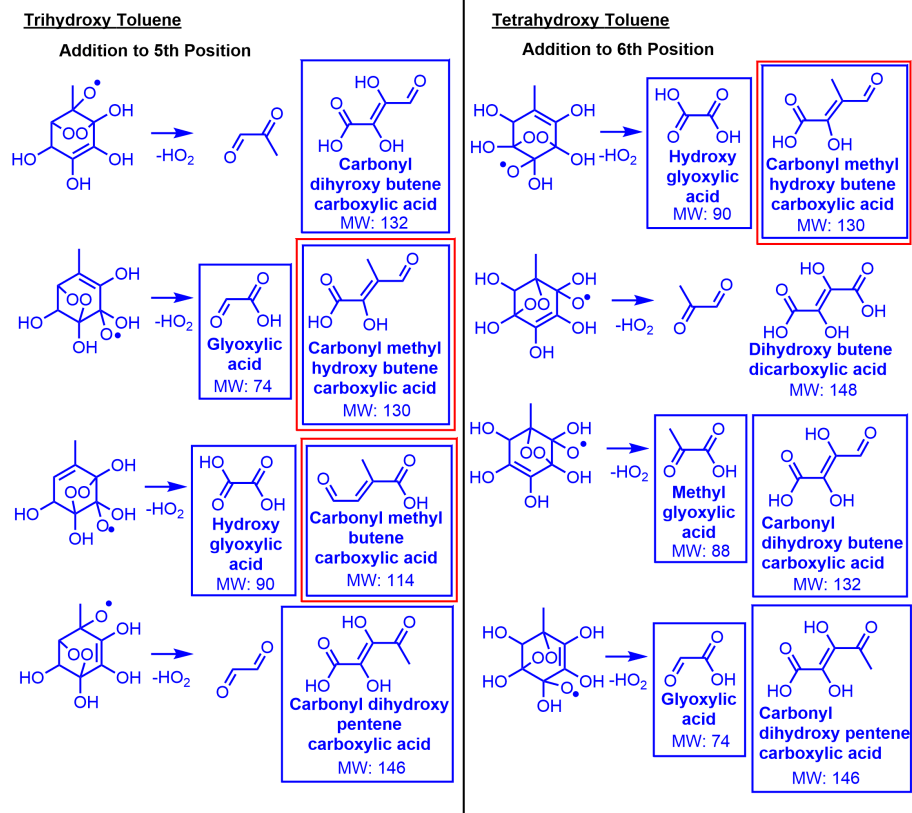
Figure 6. Proposed decomposition pathways for bicyclic intermediate compounds formed from OH oxidation of trihydroxytoluene and tetrahydroxytoluene. Blue and red boxed compounds were detected by CIMS and DART-MS, respectively.
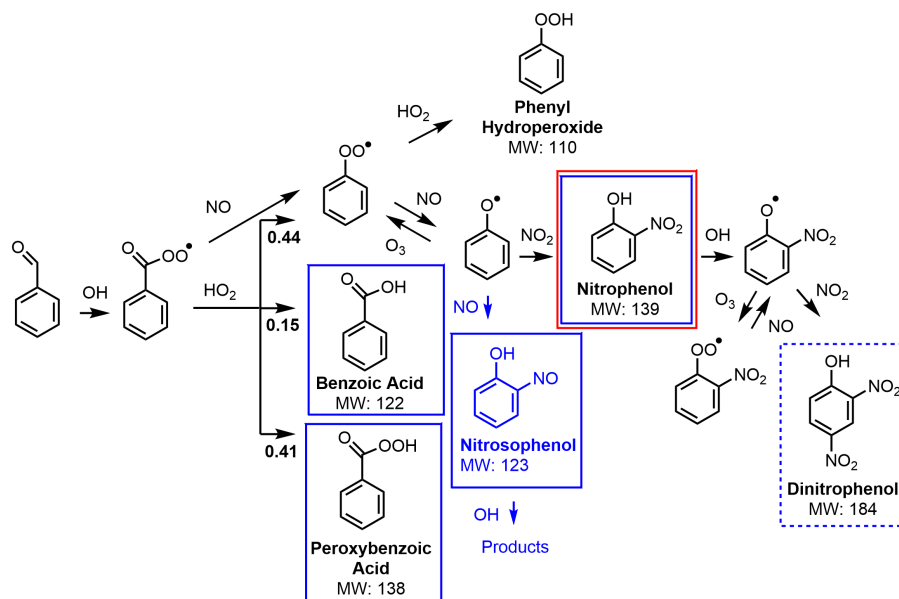
Figure 7. Gas-phase chemical mechanism for benzaldehyde photooxidation under low- and high-NO conditions. MCM v3.3.1 pathways are shown in black. Products detected by the CIMS and DART-MS are boxed in blue and red, respectively, with dashed lines indicating only a minor amount forms.
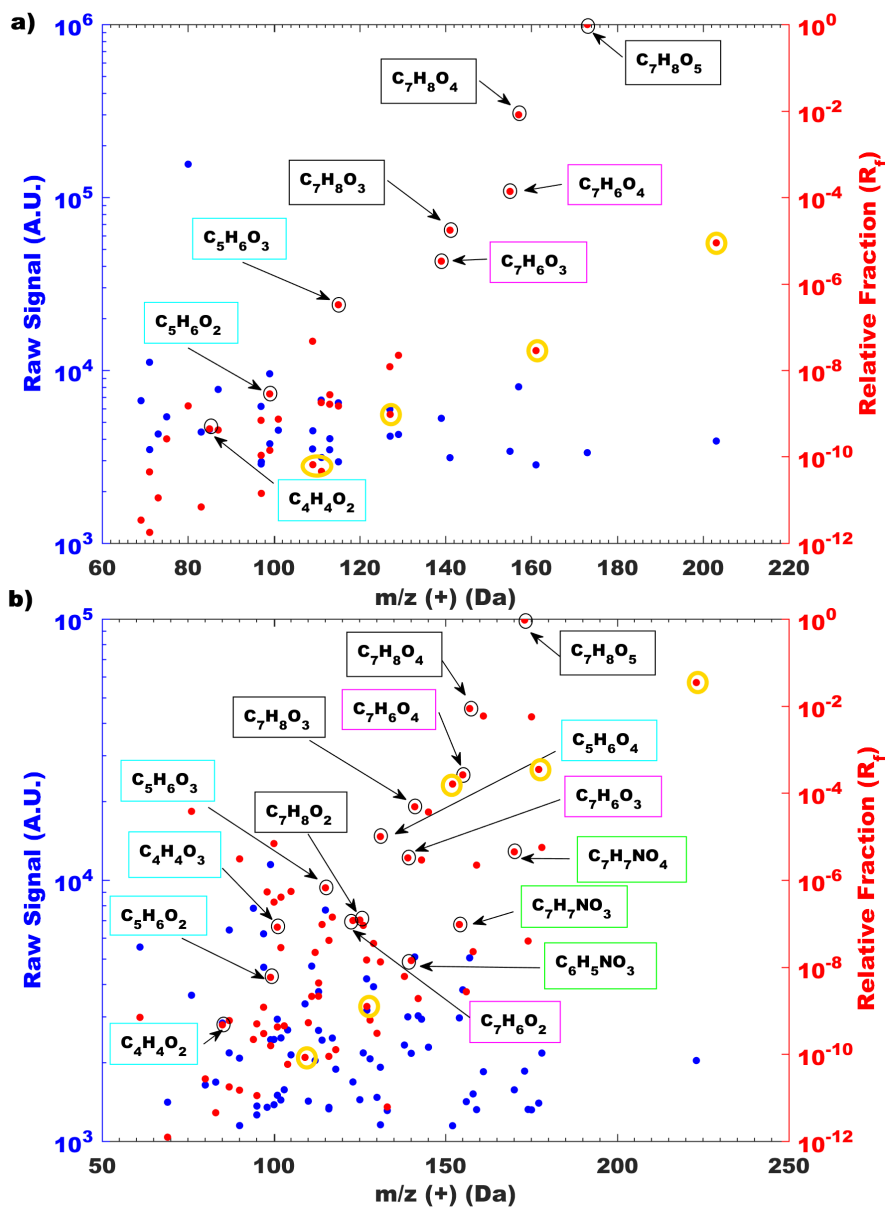
Figure 8. Particle-phase products detected by DART-MS during oxidation of toluene under low-NO conditions (a, experiment 13) and high-NO conditions (b, experiment 14) with boxes identifying the following types of compounds: polyols (black), methyl benzoquinone type compounds (magenta), decomposition products from the bicyclic intermediate pathway (cyan), nitro compounds (green), and presumed oligomerization products (i.e., those with >7 carbons, gold).
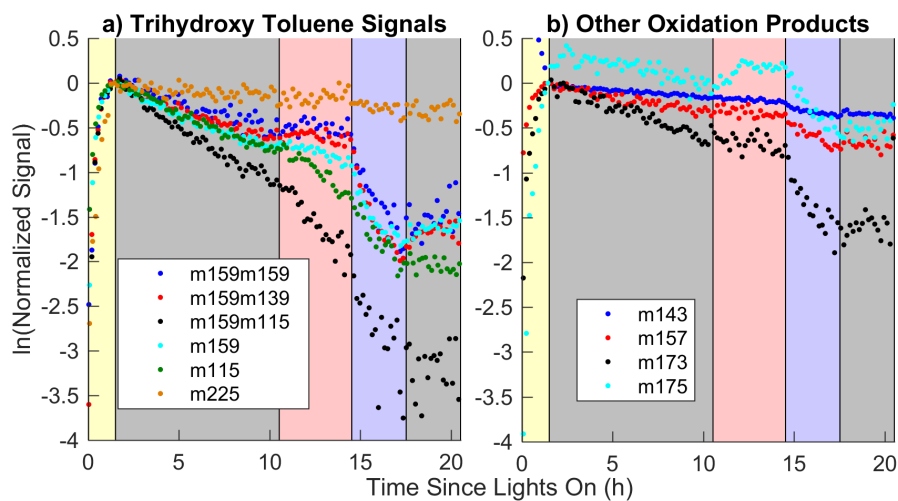
Figure 9. CIMS signals for trihydroxy toluene (panel a) and the following compounds (panel b): 3-methyl catechol (blue), hydroxy methyl benzoquinone (red), dihydroxy methyl benzoquinone (black), and tetrahydroxy toluene (cyan) during experiment 9. During this experiment, lights were turned on to generate 3-methyl catechol oxidation products (yellow shading). Then lights were turned off to measure the decay of these products to the chamber walls at 28°C (gray shading). Then the chamber was heated to 42°C (red shading), cooled to 16°C (blue shading), and finally heated back to 28°C (gray shading).
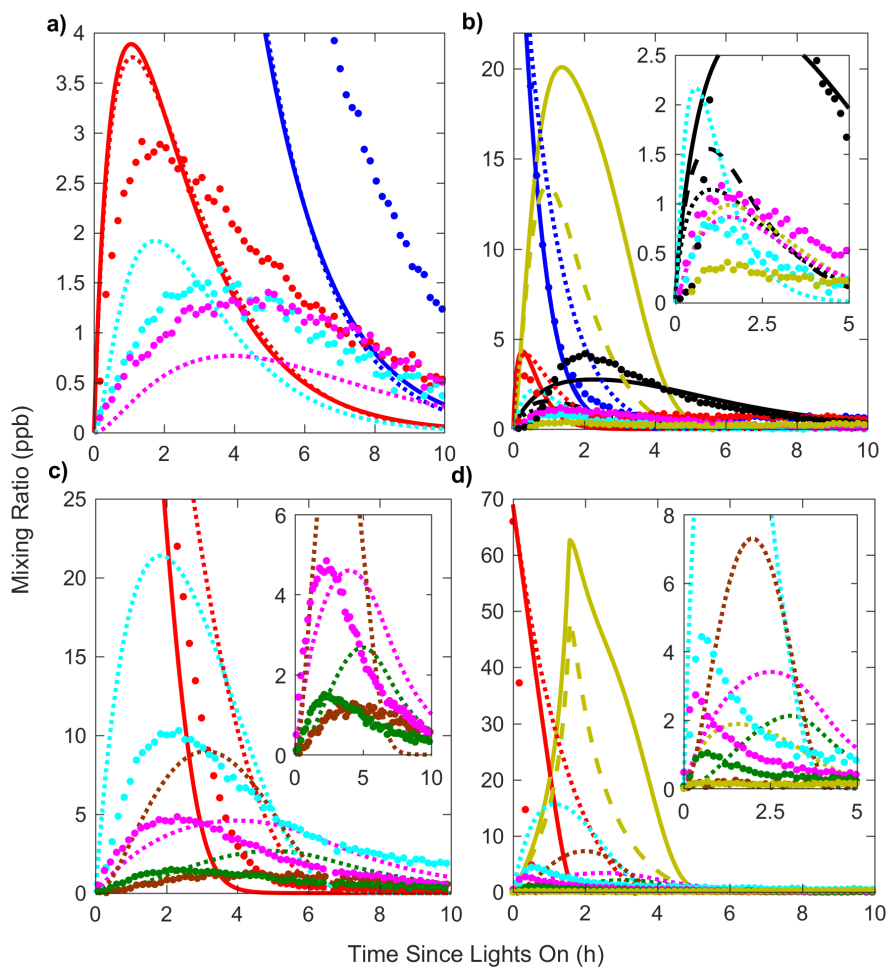
Figure 10. Kinetic model predictions (Version 1 solid lines, Version 2 dashed lines, Version 3 dotted lines) versus CIMS measurements (data points) for *o*-cresol oxidation under low-NO (a) and high-NO (b) conditions and 3-methyl catechol oxidation under low-NO (c) and high-NO (d) conditions. When necessary, a finer detail plot of selected compounds with lower signal is shown in the upper right corner. Colors for all graphs are *o*-cresol (blue), 3-methyl catechol (red), trihydroxy toluene (cyan), tetrahydroxy toluene (brown), hydroxy methyl benzoquinone (magenta), dihydroxy methyl benzoquinone (green), hydroxy nitrotoluene (black), and dihydroxy nitrotoluene (gold).

Table 1. Description of Experiments

Expt. #	VOC	VOC (ppb)	Oxidant Precursor	Initial NO (ppb)	Continuous NO Injection (ppb h^{-1}) [a]	Temp. (K)/ RH (%) [b]
			Gas-Phase Experiments [c]			
1	Toluene	98	H$_2$O$_2$ + NO	72	98 (149); 61 (223); 30 (UE)	301 / <3-7
2	Toluene	91	H$_2$O$_2$	NA	NA	301 / <3-5
3	Toluene	49	H$_2$O$_2$ + NO	74	98 (120); 61 (204); 30 (UE)	301 / <3-5
4	Toluene	46	H$_2$O$_2$	NA	NA	301 / ≤3
5	*o*-cresol	40	H$_2$O$_2$ + NO	79	98 (120); 61 (20); 30 (UE)	301 / 4-9
6	*o*-cresol	36	H$_2$O$_2$	NA	NA	301 / <3-4
7	3-methyl catechol	69	H$_2$O$_2$ + NO	74	98 (123); 30 (UE)	301 / 3-7
8	3-methyl catechol	97	H$_2$O$_2$	NA	NA	301 / ≤3
9	3-methyl catechol	59	H$_2$O$_2$	NA	NA	289-315/ <14
10	3-methyl catechol	65	H$_2$O$_2$	NA	NA	302 / <3
11	Benzaldehyde	∼50	H$_2$O$_2$	NA	NA	301 / ≤3
12	Benzaldehyde	∼50	H$_2$O$_2$ + NO	72	98 (68); 61 (35); 30 (329); 22 (UE)	301 / ≤3
			Particle-Phase Experiments [c]			
13	Toluene	286	H$_2$O$_2$	NA	NA	301 / 3-6
14	Toluene	313	H$_2$O$_2$ + NO	78	146 (263); 53 (734); 15 (UE)	300 / <3-7
15	*o*-cresol	143	H$_2$O$_2$ + NO	84	146 (262); 53 (182); 15 (UE)	301 / 9-12

[a] NO was continuously injected. The rate of NO injection decreased over the course of the experiment. The following format is used: rate in ppb h^{-1} (number of minutes injected at that rate). "UE" indicates that the rate was used until the end of the experiment. [b] RH = Relative Humidity. [c] Seed aerosol was injected into the chamber for all particle-phase experiments, but not for gas-phase experiments.

Table 2. Fraction of CIMS signal detected from the complex ion (R1) or fragment ions (transfer ion (R2) and others.)

VOC	Gas [a]	Complex	Fragments	
			Transfer	Other
o-cresol	purified air	0.77	0.12	0.11
o-cresol	dry N$_2$	0.75	0.19	0.05
3-methyl catechol	purified air	0.02	0.78	0.20
3-methyl catechol	dry N$_2$	<0.01	0.90	0.10

[a] Dry N$_2$ (RH <1%) is less humid than purified air (RH ∼1-3%).

Table 3. Estimated vapor pressures and saturation mass concentrations for main products detected by the CIMS from toluene OH oxidation

VOC	Estimated Vapor Pressure [a] (atm, 298K)		Saturation Mass Concentration [b] (C*) (μg m^{-3})	
	EVAP	Nann	Evap	Nann
Toluene	3.7×10^{-2} [c]	3.7×10^{-2} [c]	1.4×10^{8}	1.4×10^{8}
o-cresol	3.9×10^{-4} [c]	3.9×10^{-4} [c]	1.7×10^{6}	1.7×10^{6}
Acetyl acrylic acid	6.6×10^{-6}	1.7×10^{-5}	3.1×10^{4}	7.9×10^{4}
Hydroxy methyl hydroperoxy benzoquinone	1.9×10^{-9}	U	1.3×10^{1}	NA
Hydroxy methyl trioxo cyclohexene	8.2×10^{-7}	U	5.2×10^{3}	NA
3-methyl catechol	2.3×10^{-6}	6.8×10^{-6}	1.2×10^{4}	3.5×10^{4}
Hydroxy methyl benzoquinone	5.3×10^{-7}	U	3.0×10^{3}	NA
Trihydroxy toluene	1.1×10^{-8}	6.0×10^{-8}	6.3×10^{1}	3.4×10^{2}
Dihydroxy methyl benzoquinone	8.3×10^{-9}	U	5.2×10^{1}	NA
Tetrahydroxy toluene	2.4×10^{-11}	3.3×10^{-10}	1.5×10^{-1}	2.1
Trihydroxy methyl benzoquinone	9.5×10^{-11}	U	6.6×10^{-1}	NA
Pentahydroxy toluene	9.0×10^{-14}	1.1×10^{-12}	6.3×10^{-4}	7.7×10^{-3}
Hydroxy nitrotoluene	U	1.8×10^{-5}	NA	1.1×10^{5}
Hydroxy tricarbonyl pentane	3.1×10^{-4}	U	1.7×10^{6}	NA
Dihydroxy nitrotoluene	U	2.0×10^{-7}	NA	1.4×10^{3}
Glyoxylic acid	1.9×10^{-3}	U	5.5×10^{5}	NA
Benzoic acid	1.1×10^{-5}	8.2×10^{-6}	5.5×10^{4}	4.1×10^{4}
Peroxybenzoic acid	8.8×10^{-5}	U	5.0×10^{5}	NA
Nitrophenol	U	8.7×10^{-5}	NA	5.0×10^{5}
Dinitrophenol	U	3.3×10^{-7}	NA	2.5×10^{3}
Hydroxy methyl dicarbonyl butene	1.4×10^{-4}	U	6.5×10^{5}	NA
Methyl glyoxylic acid	6.1×10^{-4}	U	2.2×10^{6}	NA
Carbonyl methyl butene carboxylic acid	6.6×10^{-6}	1.9×10^{-5}	3.1×10^{4}	8.9×10^{4}
Carbonyl butene carboxylic acid	2.0×10^{-5}	3.0×10^{-5}	8.2×10^{4}	1.2×10^{5}
Carbonyl hydroxy methyl butene carboxylic acid	1.1×10^{-7}	U	5.9×10^{2}	NA
Hydroxy glyoxylic acid	2.9×10^{-7}	U	1.1×10^{3}	NA
Dicarbonyl dihydroxy pentene	5.8×10^{-6}	U	3.1×10^{4}	NA
Carbonyl hydroxy butene carboxylic acid	3.3×10^{-7}	U	1.6×10^{3}	NA
Carbonyl dihydroxy butene carboxylic acid	7.6×10^{-9}	U	4.1×10^{1}	NA
Carbonyl methyl hydroxy butene carboxylic acid	1.1×10^{-7}	U	5.9×10^{2}	NA
Carbonyl dihydroxy pentene carboxylic acid	2.4×10^{-9}	U	1.4×10^{1}	NA

[a] U = Unable to estimate, EVAP = EVAPORATION and Nann = Nannoolal. [b] Here C* = MW*P^{0} / (RT) where MW = molecular weight, P^{0} = liquid vapor pressure, R = gas constant, and T = temperature. [c] The values reported are the measured values (Yaws, 1994).